

Article

A Comparison of Evans Blue and 4-(*p*-Iodophenyl)butyryl Albumin Binding Moieties on an Integrin $\alpha_v\beta_6$ Binding Peptide

Ryan A. Davis ¹, Sven H. Hausner ², Rebecca Harris ² and Julie L. Sutcliffe ^{1,2,3,*}¹ Department of Biomedical Engineering, University of California, Davis, CA 95616, USA; rydavis@ucdavis.edu² Department of Internal Medicine, Division of Hematology/Oncology, University of California, Davis, CA 95817, USA; shhausner@ucdavis.edu (S.H.H.); relharris@ucdavis.edu (R.H.)³ Center for Molecular and Genomic Imaging, University of California, Davis, CA 95616, USA

* Correspondence: jlsutcliffe@ucdavis.edu; Tel.: +1-916-734-5536

Abstract: Serum albumin binding moieties (ABMs) such as the Evans blue (EB) dye fragment and the 4-(*p*-iodophenyl)butyryl (IP) have been used to improve the pharmacokinetic profile of many radiopharmaceuticals. The goal of this work was to directly compare these two ABMs when conjugated to an integrin $\alpha_v\beta_6$ binding peptide ($\alpha_v\beta_6$ -BP); a peptide that is currently being used for positron emission tomography (PET) imaging in patients with metastatic cancer. The ABM-modified $\alpha_v\beta_6$ -BP peptides were synthesized with a 1,4,7,10-tetraazacyclododecane-1,4,7,10-tetracetic acid (DOTA) chelator for radiolabeling with copper-64 to yield [⁶⁴Cu]Cu DOTA-EB- $\alpha_v\beta_6$ -BP ([⁶⁴Cu]1) and [⁶⁴Cu]Cu DOTA-IP- $\alpha_v\beta_6$ -BP ([⁶⁴Cu]2). Both peptides were evaluated in vitro for serum albumin binding, serum stability, and cell binding and internalization in the paired engineered melanoma cells DX3puro β_6 ($\alpha_v\beta_6$ +) and DX3puro ($\alpha_v\beta_6$ -), and pancreatic BxPC-3 ($\alpha_v\beta_6$ +) cells and in vivo in a BxPC-3 xenograft mouse model. Serum albumin binding for [⁶⁴Cu]1 and [⁶⁴Cu]2 was 53–63% and 42–44%, respectively, with good human serum stability (24 h: [⁶⁴Cu]1 76%, [⁶⁴Cu]2 90%). Selective $\alpha_v\beta_6$ cell binding was observed for both [⁶⁴Cu]1 and [⁶⁴Cu]2 ($\alpha_v\beta_6$ (+) cells: 30.3–55.8% and 48.5–60.2%, respectively, vs. $\alpha_v\beta_6$ (–) cells <3.1% for both). In vivo BxPC-3 tumor uptake for both peptides at 4 h was 5.29 ± 0.59 and $7.60 \pm 0.43\%$ ID/g ([⁶⁴Cu]1 and [⁶⁴Cu]2, respectively), and remained at 3.32 ± 0.46 and $4.91 \pm 1.19\%$ ID/g, respectively, at 72 h, representing a >3-fold improvement over the non-ABM parent peptide and thereby providing improved PET images. Comparing [⁶⁴Cu]1 and [⁶⁴Cu]2, the IP-ABM- $\alpha_v\beta_6$ -BP [⁶⁴Cu]2 displayed higher serum stability, higher tumor accumulation, and lower kidney and liver accumulation, resulting in better tumor-to-organ ratios for high contrast visualization of the $\alpha_v\beta_6$ (+) tumor by PET imaging.



Citation: Davis, R.A.; Hausner, S.H.; Harris, R.; Sutcliffe, J.L. A Comparison of Evans Blue and 4-(*p*-Iodophenyl)butyryl Albumin Binding Moieties on an Integrin $\alpha_v\beta_6$ Binding Peptide. *Pharmaceutics* **2022**, *14*, 745. <https://doi.org/10.3390/pharmaceutics14040745>

Academic Editor: Katona Gábor

Received: 1 March 2022

Accepted: 25 March 2022

Published: 30 March 2022

Publisher's Note: MDPI stays neutral with regard to jurisdictional claims in published maps and institutional affiliations.



Copyright: © 2022 by the authors. Licensee MDPI, Basel, Switzerland. This article is an open access article distributed under the terms and conditions of the Creative Commons Attribution (CC BY) license (<https://creativecommons.org/licenses/by/4.0/>).

Keywords: albumin binding moieties; peptides; Evans blue; 4-(*p*-iodophenyl)butyric acid; integrin $\alpha_v\beta_6$; integrin $\alpha_v\beta_6$ binding peptide; improved pharmacokinetics; PET imaging

1. Introduction

The use of biologically active molecules such as peptides and antibodies continues to increase for both diagnosis and therapy [1–3]. Peptides are attractive platforms for diagnostics due to their ability to achieve high target binding affinity and in part due to their small size which results in short biological half-life and rapid clearance from non-target tissues, producing good target-to-non-target contrast, low toxicity, and generally low or absent immunogenicity [1]. Synthetic advantages of peptides include simple preparation and easy, flexible functionalization or chemical modification to further improve affinity, stability, selectivity, and overall pharmacokinetic properties [1,4]. However, some of the properties that are desirable for a diagnostic agent can hamper the translation to a therapeutic, which relies on a prolonged circulation for high and persistent uptake in the targeted tissue. Too rapid clearance can render the therapeutic ineffective, and poor clearance from non-target tissue can lead to off-target toxicity. Thus, peptides typically

require fine-tuning for therapeutic applications to balance circulation time and provide high target accumulation with sufficient clearance from non-target tissues [5–7].

Chemical modifications of peptides offer a route to improving these pharmacokinetic properties; this includes incorporation of polyethylene glycol (PEG; PEGylation), glycosylation, or the formation of protein conjugates (e.g., with serum albumin) [4,8–11]. PEGylation is a convenient approach as PEGs are commercially available in a variety of molecular sizes, including mono-disperse PEGs with various functional groups for synthetic orthogonality [1,9]. PEGylation increases hydrophilicity (reducing kidney, lung, and liver accumulation) [12,13], provides increased stability (by protection from proteases), and reduces immunogenicity (by masking the peptide) [9,13]. The size and placement of the PEG on the peptides can significantly affect the pharmacokinetics and tumor accumulation [12–14]. Stability, circulation time, and tumor uptake of peptides can also be increased by chemical ligation *ex vivo* to serum albumin (taking advantage of albumin's size, long circulation time, and renal recycling) [8,15–17]. Alternatively, the same benefit can be achieved by direct attachment of a small albumin binding moiety (ABM) onto the peptide without substantially increasing the size. The ABM binds reversibly to albumin in the blood, thereby increasing circulation time and facilitating renal recycling, which, in turn, increases target tissue accumulation [8,15,16,18]. Several ABMs have been employed to modify pharmaceuticals currently used in the clinic, with some being used on their own, primarily for measuring plasma volume [16]; among the first ABMs used to modify pharmaceuticals were long-chain fatty acids, such as myristic and palmitic acid [5], and later other lipophilic molecules including benoxaprofen, phenytoin, ibuprofen, and naproxen [16].

More recently, two ABMs in particular, a fragment of Evans blue (EB) dye and the 4-(*p*-iodophenyl)butyryl (IP) group, have also been used to modify the pharmacokinetic profile of radiopharmaceuticals, in particular small molecules (folic acid and prostate specific membrane antigen (PSMA) agents) and peptides (octreotide, exendin-4, and cRGDFK) [10,11,16,18–20]. The EB-ABM was derived from Evans blue dye, a dye which has been used clinically for over 90 years to measure plasma volume and determine blood-brain barrier integrity [16,17,21]. The EB-ABM fragment was first used in 2004 as an MRI contrast agent for imaging blood vessels [22] and has since been used for a variety of applications, including determining blood volume, vascular permeability, and as a conjugate to enhance receptor targeting agents (small molecules and peptides) for both cancer imaging and therapy [9,17,23–26]. The IP-ABM has also been studied extensively to enhance radiopharmaceuticals (small molecules and peptides), where the group at the *para*-position of the aromatic ring of the IP-ABM can be tuned to adjust serum albumin affinity [15,27,28], and a neighboring aspartate residue (D) has been shown to provide a more sustained tumor retention [29]. Numerous preclinical studies have evaluated both ABMs and noted prolonged blood circulation, with an increase in tumor uptake that can also lead to a reduction of kidney accumulation [7,11,18].

The Sutcliffe laboratory has spent over a decade developing and optimizing an integrin $\alpha_v\beta_6$ -binding peptide ($\alpha_v\beta_6$ -BP) [30] to selectively target integrin $\alpha_v\beta_6$, an epithelium cell surface receptor that is absent or expressed in low levels in healthy adult epithelia, but is highly expressed in numerous challenging cancers, where it is associated with angiogenesis, proliferation, invasion, metastasis, and chemoresistance [31–41]. Thus, the integrin $\alpha_v\beta_6$ has been recognized as negative prognostic indicator with the expression levels correlating to poor prognosis and overall survival in many cancers [31–41]. During the optimization of the $\alpha_v\beta_6$ -BP, the bi-terminal PEGylation with monodispersed PEG₂₈ of the 20 amino acid A20FMDV2-peptide (NAVPNLRGDLQVLAQKVART) derived from the integrin $\alpha_v\beta_6$ -targeting foot and mouth disease virus, showed greatly improved integrin $\alpha_v\beta_6$ affinity and selectivity, and improved on the peptide's stability and tumor accumulation and retention [14]. Since then, further modifications have been tested in numerous preclinical models with an advancement of the peptide to >10-fold increase in tumor accumulation and the successful translation of the 4-[¹⁸F]fluorobenzoyl labeled [¹⁸F] $\alpha_v\beta_6$ -BP into the

clinic for PET imaging of a variety of cancers, including pancreatic adenocarcinoma [30]. Further optimization of $\alpha_v\beta_6$ -BP continues towards an integrin $\alpha_v\beta_6$ targeted peptide receptor radionuclide therapy (PRRT).

Recently, Hausner et al. described the IP-ABM modified $\alpha_v\beta_6$ -BP radiolabeled using 1,4,7-triazacyclo-nonane- N,N',N'' -triacetic acid (NOTA) for aluminum [^{18}F]fluoride chelation, with the goals of improving the biodistributions and simplifying the fluorine-18 radiochemistry [42]. The [^{18}F]AlF NOTA-IP-ABM- $\alpha_v\beta_6$ -BP had increased blood circulation and tumor accumulation that allowed for high-contrast PET imaging at 6 h post-injection (p.i.) [42], and >3.5-fold lower kidney retention than the very early generation [^{18}F]AlF NOTA-A20FMDV2-peptide [43]. Building on these data and to extend the imaging window beyond that of fluorine-18 ($t_{1/2} = 109.7$ min), a copper-64 1,4,7,10-tetraazacyclododecane-1,4,7,10-tetracetic acid (DOTA) IP-ABM- $\alpha_v\beta_6$ -BP ($t_{1/2} = 12.7$ h) was prepared, which again resulted in an increased tumor accumulation that allowed PET imaging up to 72 h p.i. [44].

In the present study, we describe a head-to-head comparison of the $\alpha_v\beta_6$ -BP modified with either EB-ABM or IP-ABM, with the goal to examine if fine tuning of the ABM could further increase tumor accumulation. Copper-64 radiolabeled [^{64}Cu]Cu DOTA-EB- $\alpha_v\beta_6$ -BP ([^{64}Cu]1) and [^{64}Cu]Cu DOTA-IP- $\alpha_v\beta_6$ -BP ([^{64}Cu]2), along with the non- $\alpha_v\beta_6$ -targeting ABM controls [^{64}Cu]Cu DOTA-EB ([^{64}Cu]3) and [^{64}Cu]Cu DOTA-IP ([^{64}Cu]4; Figure 1) were synthesized. Peptides [^{64}Cu]1 and [^{64}Cu]2 were evaluated in vitro by competitive ELISA, serum stability, albumin binding assays, and cell binding and internalization assays with DX3puro β_6 ($\alpha_v\beta_6+$), DX3puro ($\alpha_v\beta_6-$), and BxPC-3 ($\alpha_v\beta_6+$) cells (against controls [^{64}Cu]3 and [^{64}Cu]4), and in vivo by PET/CT imaging and biodistribution studies in mice bearing BxPC-3 xenograft tumors (4–72 h, p.i., against controls [^{64}Cu]3 and [^{64}Cu]4 at 4 h, p.i.).

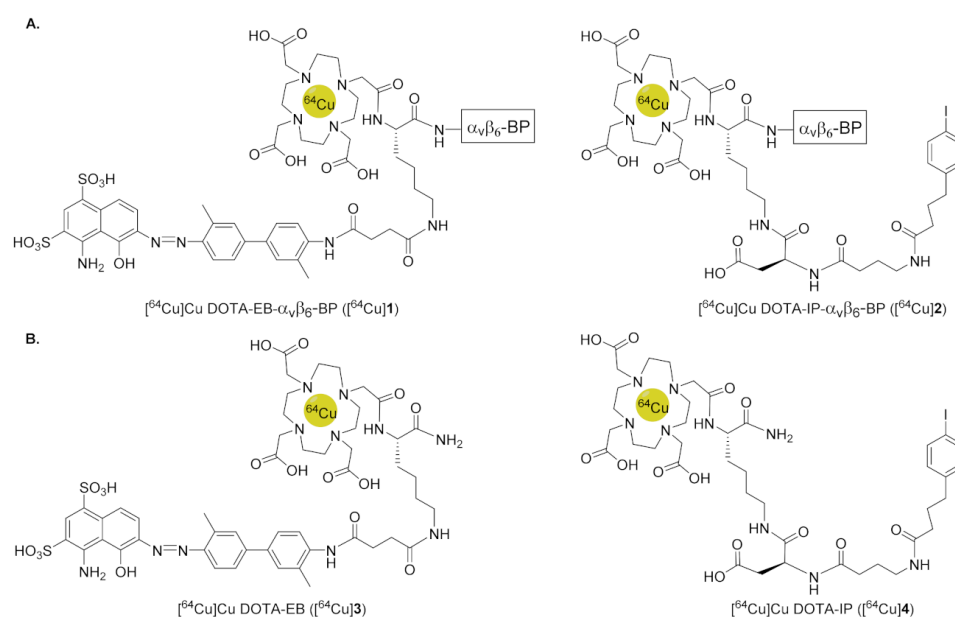


Figure 1. (A) Chemical structures of ^{64}Cu -radiolabeled-ABM- $\alpha_v\beta_6$ -BP: [^{64}Cu]Cu DOTA-EB- $\alpha_v\beta_6$ -BP and [^{64}Cu]Cu DOTA-IP- $\alpha_v\beta_6$ -BP ([^{64}Cu]1 and [^{64}Cu]2). (B) Chemical structures of ^{64}Cu -radiolabeled non-targeting-ABM controls: [^{64}Cu]Cu DOTA-EB and [^{64}Cu]Cu DOTA-IP ([^{64}Cu]3 and [^{64}Cu]4). [$\alpha_v\beta_6$ -BP = PEG₂₈-NAVPNLRGDLQVLAQRVART-PEG₂₈-CONH₂].

2. Materials and Methods

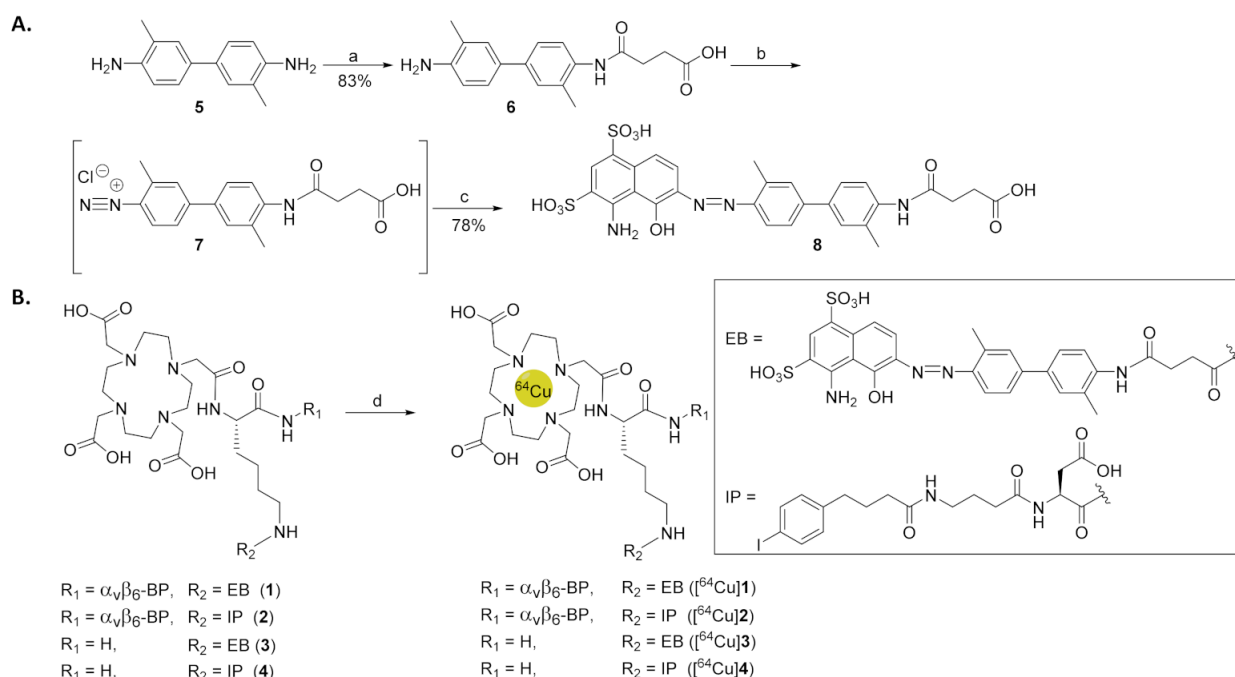
2.1. Materials and General Information

Amino acids N -terminally protected with a fluorenylmethyloxycarbonyl (Fmoc) protecting group and acid labile side chain protecting groups (trityl, Pbf, *tert*-butyl, or Boc) were purchased from Novabiochem (MA, USA) or GL Biochem (Shanghai, China). The orthogonally protected lysine with a 1-(4,4-dimethyl-2,6-dioxocyclohex-1-ylidene)-3-methylbutyl

(ivDde) sidechain protecting group and an *N*-terminal Fmoc protecting group, Fmoc-Lys(ivDde)-OH was purchased from ChemPep (Wellington, FL, USA) and the reverse ivDde-Lys(Fmoc)-OH was purchased from EMD (MA, USA). The Fmoc-NH-PEG₂₈ carboxylic acid was purchased from Polypure (Oslo, Norway) and the chelator DOTA-tris(*tert*-butyl ester) was purchased from CheMatech (Dijon, France) and Macrocylics (Plano, TX, USA). The coupling reagent 1-[bis(dimethylamino)methylene]-1*H*-1,2,3-triazolo[4,5-*b*]pyridinium 3-oxid hexafluorophosphate (HATU) was purchased from GL Biochem, and benzotriazol-1-yl-oxytripyrrolidinophosphoniumhexafluorophosphate (PyBOP) was purchased from Novabiochem. Ethylenediaminetetraacetic acid (EDTA), manganese chloride (MnCl₂), and Tris were purchased from Sigma-Aldrich (St. Louis, MO, USA). Tween 20 and sodium chloride (NaCl) were purchased from Fisher (Hampton, NH, USA). The non-fat dry milk powder was purchased from Raley's (West Sacramento, CA, USA). Anhydrous *N,N*-diisopropylethylamine (DIPEA) and hydrazine were purchased from Sigma-Aldrich and used without additional purification. Solvents *N,N*-dimethylformamide (DMF), dimethylsulfoxide (DMSO), acetonitrile (ACN), methanol (MeOH), dichloromethane (DCM), ethyl acetate (EtOAc), *n*-hexanes, and pyridine were purchased from EMD or Acros (NJ, USA). Water used was purified with a Millipore Integral 5 Milli-Q water system at 18.2 MΩ/cm resistivity through a 0.22 μm filter. All solid phase couplings were carried out by rotation in a fritted polypropylene reactor. Thin-layered chromatography (TLC) plates (silica gel 60 with 254 nm fluorescent indicator) from EMD were visualized by UV lamp at 254 nm and/or iodine staining (for the synthesis of **6**). Purification of compound **6** was carried out by normal phase flash column chromatography with silica gel (40–63 μm; Silicycle, QC, Canada). Characterization, purity, and stability were assessed by analytical C₁₂-reverse-phase (RP) high-pressure liquid chromatography (HPLC) column (Jupiter Proteo, 250 mm × 4.6 mm × 4 μm; Phenomenex, Torrance, CA, USA). A Semi-preparative C₁₈-RP-column (Proteo-Jupiter, 250 mm × 10 mm × 10 μm; Phenomenex) was used for purification as described in the Supporting Information (Table S3). All RP-HPLC were carried out on a Dionex Ultimate 3000 HPLC system or a Beckman Coulter Gold HPLC with the latter being used for all radio-RP-HPLC analysis. RP-HPLC were monitored by a UV detector at a wavelength of 220 nm; a serially connected gamma detector was used to monitor radioactivity. [⁶⁴Cu]CuCl₂ was from the University of Wisconsin Medical Physics Department (WIMR Cyclotron Labs, Madison, WI, USA). Tissue culture and cellular assays used Dulbecco's Modified Eagle Medium (DMEM), Roswell Park Memorial Institute (RPMI) 1640 medium, fetal bovine serum (FBS), bovine serum albumin (BSA), penicillin-streptomycin-glutamine (PSG), puromycin, and phosphate buffered saline (PBS; all: Gibco/Thermo Fisher). The DX3puroβ6 and DX3puro cells were a gift from Dr. John Marshall. The DX3puroβ6 and DX3puro cell lines were maintained in DMEM medium, supplemented with 10% FBS, 1% penicillin-streptomycin-glutamine, and 2 mg/mL-puromycin. The BxPC-3 cells were purchased from American Type Culture collection (ATCC, Manassas, VA, USA) and maintained in RPMI 1640 medium supplemented with 10% FBS and 1% penicillin-streptomycin-glutamine. Cells were kept in a humidified incubator at 37 °C under a 5%-carbon dioxide atmosphere. A Wizard 1470 or Wizard² 2470 automatic γ-counter (Perkin-Elmer, Waltham, MA, USA) was used to measure radioactivity samples. Mass spectrometry analysis was performed at the UC Davis Mass Spectrometry Facility using either a matrix assisted laser desorption ionization time of flight (MALDI-TOF) spectrometer (UltraFlex²; Bruker, Billerica, MA, USA) in positive ionization mode with a sinapic acid matrix (Sigma-Aldrich), or with electrospray ionization (ESI) using a quadrupole ion-trap mass spectrometer (Orbitrap; ThermoFisher). Nuclear magnetic resonance (NMR) spectra were collected at the UC Davis NMR Facility on an 800 MHz Bruker instrument with the chemical shifts referenced to the residual solvent of deuterium oxide (D₂O, HOD 4.79 ppm).

2.2. Synthesis of EB-ABM 8

The synthesis of the Evans blue fragment (EB-ABM 8) was based on previously described methods [7,17,45] (Scheme 1). In brief, *o*-toluidine 5 (531 mg, 2.5 mmol; TCI America, Inc., OR, USA) was dissolved in anhydrous pyridine (1 mL) followed by the addition of succinic anhydride (300 mg, 3.0 mmol) in DMF (1 mL) and allowed to react overnight at room temperature. The crude reaction mixture was concentrated under vacuum and purified by silica-gel column chromatography using a four solvent gradient system beginning with EtOAc/n-hexanes (1/1, *v/v*) to remove unreacted *o*-toluidine (5, yellow band). The solvent was then changed to 100% EtOAc before switching to MeOH/DCM (1/9, *v/v*) and gradually ramping to 3/7 (*v/v*) to obtain 6 (648 mg, *rt* = 0.13, 1:1 hexanes:EtOAc) as a white solid in 83% yield. Compound 6 was analyzed by analytical RP-HPLC and ESI mass spectrometry (Figure S17).



Scheme 1. (A) Synthetic route to modified EB-ABM 8. (B) Radiochemical Synthesis of [^{64}Cu]1–4. a. Succinic anhydride, DMF, pyridine (1:1), b. NaNO_2 , MeOH, $\text{HCl}/\text{H}_2\text{O}$, 0 °C, c. 1-amino-8-naphthol-2,4-disulfonic acid, NaHCO_3 , H_2O , 0 °C, d. [^{64}Cu]CuCl₂, NH_4OAc , 37 °C.

Compound 6 (300 mg, 0.96 mmol) was added to a 25 mL round bottom flask with stir bar containing MeOH (7 mL) and water (5 mL). The contents were cooled to 0 °C (ice/brine solution) and allowed to stir for 15 min prior to addition of concentrated hydrochloric acid 240 μL (HCl , 12.1 N; EMD). The diazonium formation of 7 was most successful when the addition of sodium nitrite was done in two portions; the first portion of sodium nitrite (NaNO_2 , 70 mg, 1.01 mmol; Sigma-Aldrich) was allowed to react for 5 min before the addition of the second portion (NaNO_2 , 70 mg, 1.01 mmol), after which the reaction was stirred an additional 30 min to generate 7 in situ, which was produced in better yields using the methanol co-solvent than water alone [46]. During in situ formation of 7, sodium bicarbonate (350 mg, 4.17 mmol; EMD) was dissolved in water (4 mL) with 1-amino-8-naphthol-2,4-disulfonic acid (377 mg, 1.18 mmol; TCI America, Inc.) in a separate 25 mL round bottom flask and the contents cooled in an ice/brine solution (~20 min). Next, the diazonium 7 reaction mixture (yellow) was cannulated into the 1-amino-8-naphthol-2,4-disulfonic acid (brown-purple) solution by drop-wise addition over 20 min while maintaining both solutions at 0 °C. Upon complete addition of 7, the reaction contents were allowed to stir for 3 h at 0 °C, and the crude reaction mixture was lyophilized and purified by semi-preparative RP-HPLC, and the collected material lyophilized. The EB-ABM 8 was

afforded as a fluffy purple solid (480 mg, 78%) and was analyzed by analytical RP-HPLC, ESI mass spectrometry, and NMR (Figures S18 and S19).

2.3. Synthesis of DOTA-ABM- $\alpha_v\beta_6$ -BPs 1 and 2

The $\alpha_v\beta_6$ -BP (PEG₂₈-NAVPNLRGDLQVLAQRVART-PEG₂₈) was synthesized on NovaSyn TGR resin (NovaBiochem) and PEGylation was done using monodisperse Fmoc-amino-PEG-propionic acid (Fmoc-PEG₂₈-CO₂H; FW = 1544.8 g/mol) as previously described [30] using standard Fmoc-chemistry. After each coupling or deprotection the resin was rinsed with DMF (3×), MeOH (3×), and DMF (3×). The $\alpha_v\beta_6$ -BP-resin was split in equal portions (100 mg, 0.0088 mmol) and further modified at the *N*-terminus for the synthesis of peptides 1 and 2. The DOTA-EB- $\alpha_v\beta_6$ -BP 1 was generated by first removing the *N*-terminal Fmoc of the $\alpha_v\beta_6$ -BP with 20% piperidine (Sigma-Aldrich) in DMF (2 × 10 min) followed by the addition of Fmoc-Lys(ivDde)-OH (50.6 mg, 0.088 mmol) using HATU (32.3 mg, 0.085 mmol) and DIPEA (30 μ L, 0.172 mmol) in DMF (1 mL) for 2 h. The Fmoc was subsequently removed with 20% piperidine in DMF (2 × 10 min) and DOTA-tris(*tert*-butyl ester) (50.3 mg, 0.088 mmol) was coupled for 2 h to the *N*-terminus with HATU (32.3 mg, 0.085 mmol) and DIPEA (30 μ L, 0.172 mmol) in DMF (1 mL). The removal of the ivDde lysine-sidechain protecting group was done with hydrazine (50 μ L) in DMF (1 mL, 2 × 30 min) and the resin dried under vacuum. The EB-ABM 8 (60 mg, 0.093 mmol) was then coupled to the ϵ -amine of the sidechain of the DOTA-lysine on the $\alpha_v\beta_6$ -BP-resin using PyBOP (125 mg, 0.24 mmol) and DIPEA (50 μ L, 0.287 mmol) for 6 h to yield DOTA-EB- $\alpha_v\beta_6$ -BP-resin 1 (Figure S4). The DOTA-EB- $\alpha_v\beta_6$ -BP 1 was cleaved off the resin with concomitant removal of the protecting groups using trifluoroacetic acid (TFA, 2 mL; EMD), triisopropylsilane (TIPS, 50 μ L; Alfa Aesar, Haverhill, MA, USA) and water (50 μ L), concentrated, purified, and characterized by analytical RP-HPLC and MALDI-TOF (Figure S5). The IP-ABM containing- $\alpha_v\beta_6$ -BP 2 was prepared as previously described [42,44] where upon removal the *N*-terminal Fmoc of the $\alpha_v\beta_6$ -BP-resin, a ivDde-Lys(Fmoc)-OH was coupled. Completion of DOTA-IP- $\alpha_v\beta_6$ -BP 2 was done by sequential coupling/deFmocing of (1) Fmoc-Asp(OtBu)-OH, (2) *N*- γ -Fmoc- γ -aminobutyric acid, and (3) 4-(*p*-iodophenyl)butyric acid using HATU and DIPEA for each coupling. Completion of DOTA-IP- $\alpha_v\beta_6$ -BP 2 was achieved by removal of the *N*-terminal ivDde protecting group with 5%-hydrazine in DMF followed by attachment of DOTA-tris(*tert*-butyl ester) [44]. The completed DOTA-IP- $\alpha_v\beta_6$ -BP 2 was cleaved, purified, and analyzed as described above for the DOTA-EB- $\alpha_v\beta_6$ -BP 1 (Figure S8) [44].

2.4. Synthesis of Non-Targeting ABMs 3 and 4

Using Fmoc-chemistry with Rink AM resin (200 mg, 0.114 mmol; GL Biochem), DOTA-ABM non-targeting compounds 3 and 4 were synthesized by first coupling Fmoc-Lys(ivDde)-OH (196.6 mg, 0.342 mmol) using HATU (123.5 mg, 0.325 mmol) and DIPEA (100 μ L, 0.574 mmol) in DMF (1 mL). The Fmoc was removed with 20% (*v/v*) piperidine in DMF (1 mL, 2 × 10 min) and DOTA-tris(*tert*-butyl ester) (80 mg, 0.140 mmol) was coupled for 2 h with HATU (50 mg, 0.132 mmol) and DIPEA (50 μ L, 0.287 mmol). Following the ivDde protecting group removal with hydrazine (50 μ L) in DMF (1 mL, 2 × 30 min), the resin was dried under vacuum and split into equal portions for synthesis of 3 and 4. For 3, the EB-ABM 8 (165 mg, 0.256 mmol) was coupled using PyBOP (166.5 mg, 0.32 mmol) and DIPEA (100 μ L, 0.574 mmol) for 6 h. The EB-ABM 3 was cleaved off the resin, purified, and characterized by analytical RP-HPLC and MALDI-TOF (Figure S11). IP-ABM 4 was prepared by sequential coupling/deFmocing of (1) Fmoc-Asp(OtBu)-OH (90 mg, 0.219 mmol), (2) *N*- γ -Fmoc- γ -aminobutyric acid (70 mg, 0.215 mmol), and (3) 4-(*p*-iodophenyl)butyric acid (65 mg, 0.224 mmol) using HATU (78 mg, 0.205 mmol) and DIPEA (100 μ L, 0.574 mmol) for each coupling. The IP-ABM 4 was then cleaved off the resin, purified, and characterized by analytical RP-HPLC and MALDI-TOF (Figure S14).

2.5. Radiochemical Synthesis of [⁶⁴Cu]1–4

DOTA-compounds 1–4 were dissolved in metal free water at 1 µg/µL, and the [⁶⁴Cu]CuCl₂ (1–10 µL of 0.5 M HCl, 1 and 2: 174–255.3 MBq, 3 and 4: 51–55 MBq) was diluted with 1.0 M ammonium acetate (NH₄OAc, Sigma-Aldrich) aqueous solution (pH = 8.0) to 0.27 µL/MBq. Peptides 1 and 2 were added to the NH₄OAc buffered [⁶⁴Cu]CuCl₂ such that the starting molar activity of the reaction was between 18.5 and 20 GBq/µmol. The starting molar activity for compounds 3 and 4 was between 15.9 and 17.1 GBq/µmol. The reaction mixtures were vortexed and warmed to 37 °C for 30 min. The radiochemical purity was assessed by quenching an aliquot of the reaction (≤1 µL; 0.74–3.7 MBq) with 0.1 M EDTA (50 µL) and analyzed by analytical RP-HPLC. Product identity was confirmed by cold spike RP-HPLC, i.e., co-injection of the radiolabeled product with authenticated respective [^{Nat}Cu]Cu 1–4 reference standard of each compound (Figures S6, S9, S12 and S15). [^{Nat}Cu]Cu 1–4 reference standards were produced via reaction of DOTA-compounds 1–4 (0.1–0.5 mg) with excess CuCl₂ (Sigma-Aldrich, 1–6 mg) in water (50 µL) for 30 min at room temperature, and purified directly by RP-HPLC and confirmed by MALDI-TOF (Figures S7, S10, S13 and S16).

2.6. Integrin α_vβ₆ Affinity ELISA

Affinity for the integrin α_vβ₆ was determined by competitive binding ELISA of [^{Nat}Cu]1 and [^{Nat}Cu]2 against biotinylated-LAP (G&P Biosciences, Santa Clara, CA, USA) as previously described to determine the half-maximum inhibitory concentration (IC₅₀) [44]. Briefly, in a 96 well Nunc Immuno maxisorp plate, capturing anti-α_v antibody (P2W7, 5 µg/mL, Abcam, MA, USA) was plated (50 µL/well) at 37 °C for 1 h, washed with PBS (3×), and blocked overnight with blocking buffer (300 µL/well, 0.5% non-fat dry milk powder (*w/v*), 1% Tween 20, in PBS). It was then washed with wash buffer that consisted of 2 mmol/L of Tris buffer (pH = 7.6), 150 mmol/L sodium chloride, 1 mmol/L manganese chloride, and 0.1% Tween 20 (*v/v*) in deionized water (3×). Purified integrin α_vβ₆ (R&D Systems, Minneapolis, MN, USA) in conjugate buffer (50 µL/well, 20 mM Tris, 1 mM MnCl₂, 150 mM NaCl, 0.1% Tween, 0.1% milk powder in water) was then added to each well, incubated at 37 °C for 1 h, followed by washing using wash buffer 3×. Serial dilutions of each peptide stock of 2 mmol/L in 10% DMSO (*v/v*) into PBS and biotinylated natural ligand LAP were premixed in equal volumes and placed onto the plate in triplicate for each peptide concentration (50 µL/well) and allowed to incubate at 37 °C for 1 h then washed with wash buffer (3×). A 1:1000 dilution of ExtrAvidin Horseradish Peroxidase (HRP; Fisher, NH, USA) was added to each well (50 µL/well), incubated at 37 °C for 1 h, and then washed with wash buffer (3×). The ExtrAvidin HRP was detected with TMB One solution (50 µL/well; Promega Corp., Madison, WI, USA) for 10–15 min at room temperature. The reaction was stopped by adding 1N sulfuric acid (H₂SO₄, 50 µL/well; EMD, MA, USA) and the absorbance was measured in a Multiscan Ascent plate reader (Thermo Fisher, Waltham, MA, USA) at 450 nm. Half-maximal inhibitory concentration (IC₅₀) of peptides was determined by fitting to sigmoidal dose-response model in GraphPad Prism 8.0 (GraphPad, CA, USA). For the positive control no peptide was added and for the negative controls either no biotinylated-LAP or no integrin α_vβ₆ was added.

2.7. Cell Binding and Internalization Assay

Binding of [⁶⁴Cu]1–4 and internalization to DX3puro, DX3puroβ6, and BxPC-3 cells were determined as previously described [44]. Prior to the experiment, the cells were analyzed by flow cytometry to confirm levels of integrin α_vβ₆ expression. Non-fat dry milk powder (0.5% *w/v* in PBS) was used to pretreat the assay tubes to prevent non-specific binding. Aliquots of [⁶⁴Cu]1–4 (≤1 µL, 7.4–18.5 KBq) in 50 µL serum free medium (pH 7.2) were added to a cell suspension (3.75 × 10⁶ cells in 50 µL serum free medium) and incubated for 1 h at room temperature in closed microfuge tubes (*n* = 3/cell line/compound) and gently agitated every 3 min to ensure mixing. The cells were pelleted by centrifugation at 200 (RCF) for 3 min and the supernatant collected. The cell pellet was washed with 0.5 mL

serum free medium and the wash medium combined with the original supernatant. The cells were resuspended in 0.6 mL serum free medium for γ -counting. The fraction of bound radioactivity was determined with a γ -counter (by measuring cell pellet and combined supernatants). To determine the fraction of internalized radioactivity, the cells were re-pelleted, and re-suspended in acidic wash buffer (0.2 mol/L sodium acetate, 0.5 mol/L sodium chloride, pH 2.5, 300 μ L, 4 $^{\circ}$ C, 5 min) to release surface-bound activity, followed by a wash with PBS (300 μ L). The internalized fraction was determined with a γ -counter (cell pellet vs. radioactivity released into supernatant).

2.8. Human and Mouse Serum Binding Assay and Stability Assay

Serum protein binding of [64 Cu]1 and [64 Cu]2 was assessed following the previously reported method [42]. Peptides [64 Cu]1 and [64 Cu]2 were evaluated by ultrafiltration using Centrifree Ultrafiltration devices (EMD) according to the manufacturer's recommendations. Experiments were carried out in triplicate. The Centrifree Ultrafiltration devices were pretreated with PBS containing Tween 20 (5% *v/v*), followed by triplicate rinses with PBS. An aliquot of each peptide [64 Cu]1 or [64 Cu]2 in PBS (≤ 25 μ L, 20–60 KBq) was thoroughly mixed with 0.5 mL of serum at 37 $^{\circ}$ C in a microfuge tube. The mixture was incubated at 37 $^{\circ}$ C for 5 min, and an aliquot (50 μ L) was transferred to a tube for γ -counting. The remaining sample was transferred to a Centrifree Ultrafiltration device and centrifuged for 40 min at 1500 (RCF) at ambient temperature (20–24 $^{\circ}$ C). An aliquot (50 μ L) of the filtrate was transferred to a tube for γ -counting. For each radiolabeled peptide, a blank was run using 0.5 mL PBS/Tween 20 (5% *v/v*) instead of serum ($n = 3$) to determine non-specific binding. Following γ -counting, the protein-bound radioactivity was calculated by subtracting the counts measured in the filtrate aliquot (i.e., not protein-bound) from the counts in the corresponding serum aliquot. The data are expressed as mean \pm standard deviation of fraction of radioactivity bound to protein after subtraction of non-specific binding determined in the blank.

For serum stability, mouse serum or human serum (0.5 mL, both purchased from Sigma-Aldrich) was combined with an aliquot of each of the peptides [64 Cu]1 and [64 Cu]2 (≤ 25 μ L, 14.8–22.2 MBq) and incubated at 37 $^{\circ}$ C. At each time point (1, 4, and 24 h) an aliquot (50–200 μ L) was taken, proteins precipitated with ethanol, and removed by pelleting at 1500 (RCF) for 4 min. The ethanol solution was diluted with water (1 mL) and analyzed by RP-HPLC as previously described [47].

2.9. Biodistribution

All animal procedures conformed to the Animal Welfare Act and were approved by the University of California, Davis Institutional Animal Care and Use Committee. Female athymic nu/nu-nude mice (6–8 weeks old) were purchased from Charles River Laboratories (Wilmington, MA, USA) and provided food and water on an ad libitum basis. BxPC-3 xenografts were implanted according to previous methods [42,44]. Briefly, BxPC-3 cells were evaluated by flow cytometry to confirm integrin $\alpha_v\beta_6$ expression levels, injected subcutaneously into the left flank [5 million in 100 μ L of a 1:1 mixture of serum-free RPMI and GFR Matrigel (Corning, New York, NY, USA)], and allowed to grow for approximately 3 weeks until tumors reached a diameter of 0.5–1 cm.

For biodistribution studies the [64 Cu]1–4 (3.7–5.55 MBq) in PBS (100 μ L, pH 7.2) was injected intravenously (i.v.) via catheter into the tail vein. Following a conscious uptake period, the mice were anesthetized (5% isoflurane), euthanized, and dissected ([64 Cu]1 and [64 Cu]2, $n = 3$ /radiolabeled peptide/time point; 4, 24, and 48 h p.i.; the 72 h time point was obtained from the imaging animals after the 72 h PET/CT scans; compounds [64 Cu]3 and [64 Cu]4, $n = 2$ /radiolabeled compound at 4 h p.i.). Tissues were rapidly collected, weighed, and radioactivity measured with a γ -counter. Decay-corrected radioactivity concentrations are expressed as the percentage of injected dose per gram of tissue (% ID/g). Data are reported as mean \pm standard deviation (SD) (Figure S20, S21 and S25).

2.10. Blocking Biodistribution

For blocking studies, the metal free peptides **1** or **2** (~220 nmol, 1.3 mg in 100 μ L PBS), respectively, were injected i.v. ($n = 1$ /peptide) as described above 10 min prior to the injection of matching radiolabeled [^{64}Cu]**1** or [^{64}Cu]**2** (3.7–5.55 MBq, 100 μ L PBS). After a conscious 4 h uptake period, the animals were anesthetized, sacrificed, tissues rapidly collected, and analyzed as described above. Decay-corrected radioactivity concentrations are expressed as a percentage of injected dose per gram of tissue (% ID/g) (Figure S23).

2.11. PET-Imaging

For imaging studies, [^{64}Cu]**1** and [^{64}Cu]**2** (7.77–8.88 MBq) in PBS (100 μ L, pH 7.2) were injected i.v. via a catheter into the tail vein of mice ($n = 3$ /radiolabeled peptide) anesthetized with 2–3% isoflurane in medical grade oxygen. Animals were imaged in a prone position two at a time side by side. PET/CT scans were acquired using Inveon scanners (Inveon DPET scanner and Inveon SPECT/CT scanner, Siemens Medical Solutions, Knoxville, TN, USA; PET scans: a static 15 min scan at 4 h p.i., static 30 min scans at 24 and 48 h p.i., and a static 1 h scan at 72 h p.i.) and analyzed as previously described using the Inveon Research Workplace software (Siemens) [42,44].

2.12. Statistical Analysis

Quantitative data are reported as mean \pm standard deviation (SD). Statistical significance was determined by a paired two-tailed Student's *t*-test from the two independent sample means to give a significance value (*p*-value) at 95% confidence interval (CI). A *p*-value of <0.05 was considered statistically significant.

3. Results

3.1. Synthesis of EB-ABM **8**

EB-ABM **8** was generated efficiently in three synthetic steps from *o*-tolidine **5** in an overall yield of 65% (Scheme 1A). EB-ABM **8** was characterized by analytical RP-HPLC with a retention time of 17.72 min; ESI-MS m/z [$\text{M} + \text{H}$] $^+$ for $\text{C}_{28}\text{H}_{27}\text{N}_4\text{O}_{10}\text{S}_2$ calc'd 643.1163; found 643.1207, and by ^1H NMR (Figures S18 and S19). ^1H NMR (800 MHz, D_2O) δ 8.28 (s, 1H), 7.55 (d, $J = 9.4$ Hz, 1H), 7.29–7.27 (m, 2H), 7.24–7.23 (m, 1H), 7.17–7.16 (m, 1H), 7.13–7.12 (m, 1H), 6.98–6.97 (m, 1H), 6.88 (d, 7.8 Hz, 1H), 2.64–2.61 (m, 4H), 2.12 (s, 3H), 1.96 (s, 3H).

3.2. Synthesis and Radiochemical Synthesis of [^{64}Cu]**1–4**

DOTA-compounds **1–4** were prepared in >97% isolated purity after RP-HPLC purification. DOTA-EB- $\alpha_v\beta_6$ -BP **1** had an RP-HPLC retention time of 17.22 min with a MALDI-TOF m/z [$\text{M} + \text{Na}$] $^+$ for $\text{C}_{261}\text{H}_{460}\text{N}_{46}\text{NaO}_{102}\text{S}_2$ calc'd 5958.1556; found 5958.1756 (Figure S5). DOTA-IP- $\alpha_v\beta_6$ -BP **2** had an RP-HPLC retention time of 17.07 min with a MALDI-TOF m/z [$\text{M} + \text{H}$] $^+$ for $\text{C}_{251}\text{H}_{458}\text{IN}_{44}\text{O}_{98}$ calc'd 5786.1314; found 5786.1209 (Figure S8). DOTA-EB-ABM **3** had an RP-HPLC retention time of 14.18 min with a MALDI-TOF m/z [$\text{M} + \text{H}$] $^+$ for $\text{C}_{50}\text{H}_{66}\text{N}_{11}\text{O}_{17}\text{S}_2$ calc'd 1156.4074; found 1156.4079 (Figure S11). DOTA-IP-ABM **4** had an RP-HPLC retention time of 14.46 min with a MALDI-TOF m/z [$\text{M} + \text{H}$] $^+$ for $\text{C}_{40}\text{H}_{63}\text{IN}_9\text{O}_{13}$ calc'd 1004.3585; found 1004.3590 (Figure S14).

The ^{64}Cu -radiolabeled compounds ([^{64}Cu]**1–4**) were produced in near quantitative yields ($n = 2–4$ /compound/molar activity ranging between 16 and 20 GBq/ μmol) by reaction of with [^{64}Cu] CuCl_2 in 1.0 M NH_4OAc -buffer (pH = 8) at 37 $^\circ\text{C}$ for 30 min (Scheme 1B). The radiochemical purities were $\geq 97\%$ as determined analytical radio-RP-HPLC and compounds [^{64}Cu]**1–4** used without further purification. Analytical radio-RP-HPLC retention times were: [^{64}Cu]**1**—19.05 min (Figure S6); [^{64}Cu]**2**—18.68 min (Figure S9); [^{64}Cu]**3**—17.01 min (Figure S12); and [^{64}Cu]**4**—16.73 min (Figure S15).

3.3. Integrin $\alpha_v\beta_6$ Affinity ELISA

Competitive ELISA against biotinylated LAP, demonstrated that both ABM modifications of $\alpha_v\beta_6$ -BP were well tolerated; [^{64}Cu]1 and [^{64}Cu]2 showed high integrin $\alpha_v\beta_6$ -affinity as expressed by the half-maximum inhibitory concentrations (IC_{50}); [^{64}Cu]1 and [^{64}Cu]2: $\text{IC}_{50} = 14 \pm 2$ and 19 ± 5 nM, respectively) compared to DOTA- $\alpha_v\beta_6$ -BP ($\text{IC}_{50} = 28 \pm 3$ nM) [44].

3.4. Cell Binding and Internalization Assay

Cell binding studies showed that [^{64}Cu]1 and [^{64}Cu]2 both bound to cells in an $\alpha_v\beta_6$ -dependent manner at similar levels (DX3puro β_6 (+): [^{64}Cu]1 $55.8 \pm 3.0\%$ of total radioactivity, [^{64}Cu]2 $60.2 \pm 3.9\%$; BxPC-3 (+): [^{64}Cu]1 $30.3 \pm 2.7\%$, [^{64}Cu]2 $48.5 \pm 3.5\%$; and the negative control DX3puro (-): [^{64}Cu]1 $2.7 \pm 0.5\%$, [^{64}Cu]2 $3.1 \pm 0.3\%$, Figure 2). This resulted in binding ratios for DX3puro β_6 (+) vs. DX3puro (-) of 20.7:1 for [^{64}Cu]1 and 19.4:1 for [^{64}Cu]2. Internalization into $\alpha_v\beta_6$ -positive cells was also high ([^{64}Cu]1: 48.5–52.7% of the bound radioactivity, [^{64}Cu]2: 41.5–54.8%, Figure 2). The non-targeting control ABM conjugates [^{64}Cu]3 and [^{64}Cu]4 exhibited low, non-specific binding to all cell lines ($\leq 4.3\%$; Figure S24).

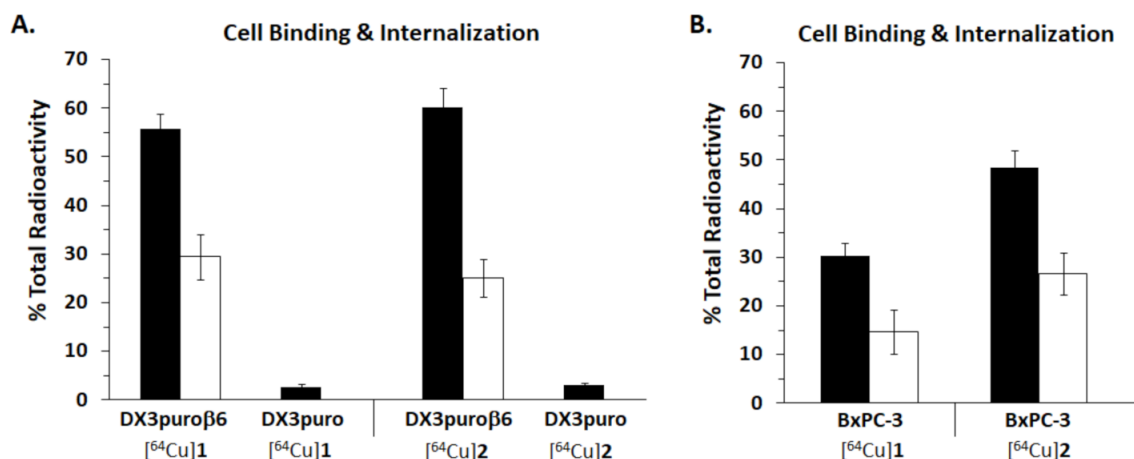


Figure 2. Cell binding (■) and internalization (□) for [^{64}Cu]Cu DOTA-EB- $\alpha_v\beta_6$ -BP ([^{64}Cu]1) and [^{64}Cu]Cu DOTA-IP- $\alpha_v\beta_6$ -BP ([^{64}Cu]2) for (A) DX3puro β_6 ($\alpha_v\beta_6$ +) and DX3puro ($\alpha_v\beta_6$ -) cells and (B) BxPC-3 ($\alpha_v\beta_6$ +) cells.

3.5. Human and Mouse Serum Binding Assay and Stability Assay

Serum albumin binding for [^{64}Cu]1 and [^{64}Cu]2 was similar, with higher binding to human serum protein ($53.4 \pm 0.9\%$ and $63.3 \pm 1.5\%$, respectively) than to mouse serum protein ($41.9 \pm 1.1\%$ and $44.0 \pm 0.1\%$, respectively; Figure 3A). The ABM modifications of [^{64}Cu]1 and [^{64}Cu]2 increased the serum albumin affinity as the [^{64}Cu]Cu DOTA- $\alpha_v\beta_6$ -BP without an ABM modification showed $<29\%$ binding to either serum albumin [44]. Both peptides showed high stability in human serum at 37°C ([^{64}Cu]1 1 h: 99% and 4 h: 89% intact; [^{64}Cu]2 1 h: 99% and 4 h: 93% intact) with some degradation apparent after 24 h ([^{64}Cu]1: 76% intact vs. [^{64}Cu]2: 90% intact, Figure 3B). In contrast, faster degradation was observed in mouse serum at 37°C , and the stability was lower for [^{64}Cu]1 than for [^{64}Cu]2 at all-time points; [^{64}Cu]1 was 78% intact at 1 h, dropping to 58% at 4 h, and largely metabolized at 24 h (14% intact). By comparison, [^{64}Cu]2 was 92% and 83% intact at 1 h and 4 h, respectively, with 48% remaining intact at 24 h, a 3.4-fold higher stability than [^{64}Cu]1 (Figure 3C).

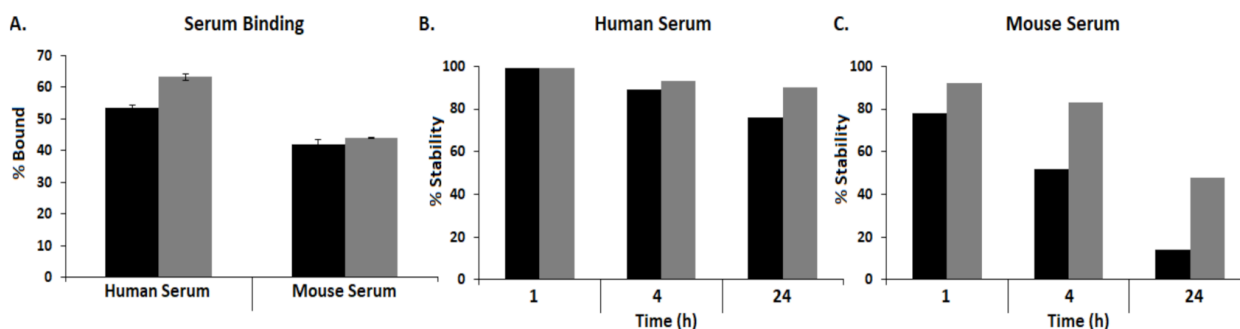


Figure 3. (A) Binding to human and mouse serum ($n = 3$ /compound/condition; bars: SD). (B) Stability in human serum at 37 °C. (C) Stability in mouse serum at 37 °C for [^{64}Cu]1 (■) and [^{64}Cu]2 (▒).

3.6. Biodistribution

The biodistributions for [^{64}Cu]1 and [^{64}Cu]2 in the BxPC-3 tumor model showed good tumor uptake (4 h to 72 h: [^{64}Cu]1 5.29 ± 0.59 to $3.32 \pm 0.46\%$ ID/g, [^{64}Cu]2 7.60 ± 0.43 to $4.91 \pm 1.19\%$ ID/g, Figure 4). Overall, tumor uptake of [^{64}Cu]2 appeared higher than of [^{64}Cu]1, particularly at the earliest time point, and relative tumor washout over the total observed time frame was similar for both peptides. The ABM modifications increased tumor accumulation by >3- to 4.5-fold compared to the [^{64}Cu]Cu DOTA- $\alpha_v\beta_6$ -BP without an ABM, which had only $1.61 \pm 0.70\%$ ID/g at 4 h in the same BxPC-3 tumor model [44]. Clearance for [^{64}Cu]1 and [^{64}Cu]2 was primarily renal and the kidneys were the organ with the highest levels of radioactivity (Figure S20 and S21). Notably, [^{64}Cu]1 showed more than double the kidney uptake of [^{64}Cu]2 at 4 h, p.i. ([^{64}Cu]1 $75.51 \pm 7.26\%$ ID/g; [^{64}Cu]2 $33.56 \pm 5.39\%$ ID/g; $p = 0.0013$) and remained significantly higher for at least 48 h (>1.7-fold, $p < 0.05$), but both were cleared from the kidneys over time with accumulation dropping at 72 h ([^{64}Cu]1 $19.97 \pm 6.91\%$ ID/g; [^{64}Cu]2 $11.48 \pm 1.02\%$ ID/g; $p = 0.103$, Figure 4). Kidney accumulation for the ABM containing peptides [^{64}Cu]1 and [^{64}Cu]2 was initially higher than for the parent non-ABM containing [^{64}Cu]Cu DOTA- $\alpha_v\beta_6$ -BP ($20.37 \pm 1.67\%$ ID/g at 4 h to $6.81 \pm 1.36\%$ ID/g at 48 h) [44]. Some clearance for [^{64}Cu]1 and [^{64}Cu]2 was also observed through the gastrointestinal tract (GI), with the stomach having the highest uptake at 4 h, p.i. ([^{64}Cu]1: stomach $6.41 \pm 0.64\%$ ID/g, small intestines $4.72 \pm 0.55\%$ ID/g, large intestines $4.13 \pm 0.10\%$ ID/g, [^{64}Cu]2: stomach $18.07 \pm 2.91\%$ ID/g, small intestines $9.55 \pm 1.21\%$ ID/g, large intestines $9.83 \pm 0.69\%$ ID/g; Figure 4). Clearance from the GI tract was further confirmed by radioactivity measurements of fecal matter (4–72 h: [^{64}Cu]1: 3.03 ± 0.67 to $1.81 \pm 0.74\%$ ID/g; [^{64}Cu]2: 9.32 ± 1.08 to $2.29 \pm 0.53\%$ ID/g; Figure 4). The GI uptake for [^{64}Cu]2 was more than double that of [^{64}Cu]1 at the earliest time point, but both peptides dropped over time to below 3.2% ID/g at 72 h. The liver uptake was moderate (<3% ID/g) throughout for both peptides; but it increased to significantly higher levels for the EB-ABM containing peptide [^{64}Cu]1, beginning at 24 h, reaching >1.8-fold higher levels than [^{64}Cu]2 at 72 h ($2.36 \pm 0.51\%$ ID/g vs. $1.30 \pm 0.13\%$ ID/g, respectively; $p = 0.025$, Figure 4). Overall, the EB-ABM containing peptide [^{64}Cu]1 had a less favorable pharmacokinetic profile with significantly higher uptake in the kidneys and liver, resulting in generally lower tumor-to-tissue ratios for [^{64}Cu]1 compared to [^{64}Cu]2, most notably for the tumor-to-kidney ratio ([^{64}Cu]1 $0.13 \pm 0.06/1$ to $0.19 \pm 0.08/1$ vs. [^{64}Cu]2 $0.20 \pm 0.06/1$ to $0.44 \pm 0.14/1$), and the tumor-to-liver ratio ([^{64}Cu]1 $2.39 \pm 0.59/1$ to $1.47 \pm 0.47/1$ vs. [^{64}Cu]2 $2.72 \pm 0.62/1$ to $3.77 \pm 0.72/1$) (Figure S22).

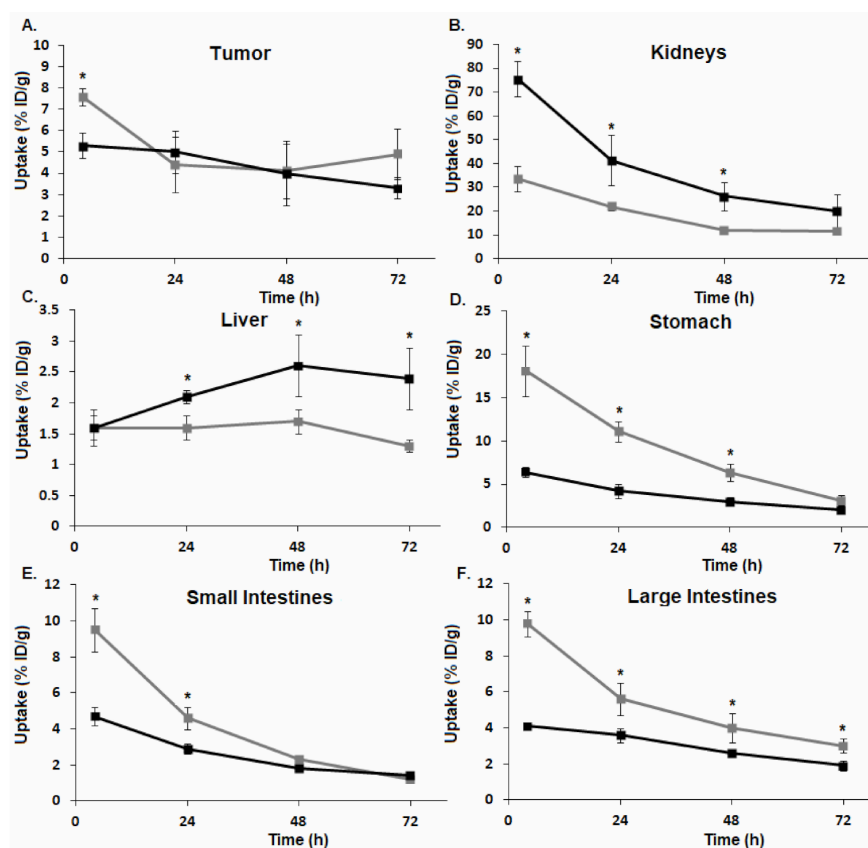


Figure 4. Biodistribution time activity plots for $[^{64}\text{Cu}]1$ (■) and $[^{64}\text{Cu}]2$ (■). (A) BxPC-3 tumors. (B) kidneys. (C) liver. (D) stomach. (E) small intestines. (F) large intestines (* $p \leq 0.05$).

The non- $\alpha_v\beta_6$ -targeting ABM controls $[^{64}\text{Cu}]3$ and $[^{64}\text{Cu}]4$ were used to determine non-specific uptake and provide support that the enhanced tumor accumulation of ABM containing peptides $[^{64}\text{Cu}]1$ and $[^{64}\text{Cu}]2$ was due to integrin $\alpha_v\beta_6$ receptor mediated uptake. The biodistributions of the non- $\alpha_v\beta_6$ -targeting ABM controls $[^{64}\text{Cu}]3$ and $[^{64}\text{Cu}]4$ at 4 h p.i. ($n = 2/\text{compound}$) showed prolonged blood circulation with much higher blood accumulation ($38.9 \pm 10.4\%$ ID/g and $9.5 \pm 1.3\%$ ID/g, respectively; Figure 5, Figure S25). This increased blood accumulation also led to higher systemic accumulation in other tissues, especially the highly perfused tissues such as the heart, muscle, liver, and lung (Figure 5, Figure S25), with the exception of the kidneys ($18.6 \pm 1.4\%$ ID/g and $4.34 \pm 0.61\%$ ID/g, respectively). These distinctly different pharmacokinetic profiles of the non-integrin $\alpha_v\beta_6$ -targeting $[^{64}\text{Cu}]3$ and $[^{64}\text{Cu}]4$ resulted in a low tumor-to-blood ratio of $<0.9/1$ compared to $>4/1$ for $[^{64}\text{Cu}]1$ and $[^{64}\text{Cu}]2$, a lower tumor-to-muscle ratio ranging from 5.6 to 6.3/1 for $[^{64}\text{Cu}]3$ and $[^{64}\text{Cu}]4$ compared to $>8/1$ for $[^{64}\text{Cu}]1$ and $[^{64}\text{Cu}]2$, and a lower tumor-to-liver ratio of 1.2–1.3/1 for $[^{64}\text{Cu}]3$ and $[^{64}\text{Cu}]4$ compared to 3.2–4.9/1 for $[^{64}\text{Cu}]1$ and $[^{64}\text{Cu}]2$ (Figure 5, Figure S26).

3.7. Blocking Biodistribution

Integrin $\alpha_v\beta_6$ -dependence of the tumor uptake was further substantiated by blocking studies with pre-administration of the respective nonradioactive peptide, which reduced tumor uptake to 2.91% ID/g and 2.89% ID/g for $[^{64}\text{Cu}]1$ and $[^{64}\text{Cu}]2$, respectively (4 h; $\Delta = -45\%$ and -62% , $p = 0.0124$ and 0.0007 , respectively; Figure S23).

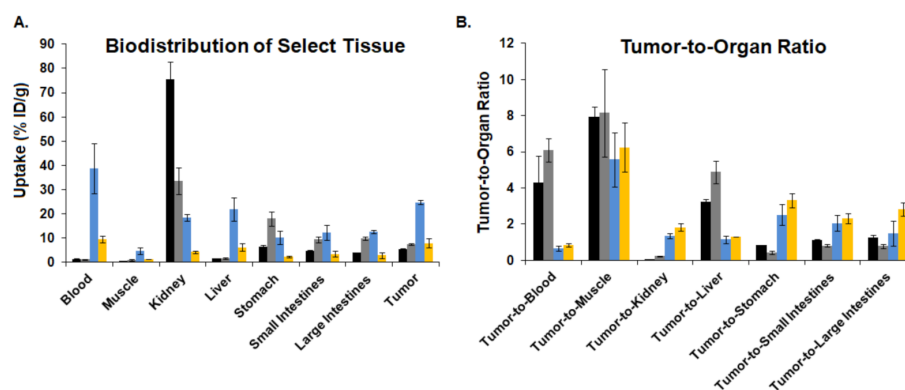


Figure 5. (A) Biodistribution of select tissues at 4 h p.i. for $[^{64}\text{Cu}]1-4$. (B) Tumor-to-organ ratios at 4 h p.i. for $[^{64}\text{Cu}]1-4$ $[^{64}\text{Cu}]1$ (■), $[^{64}\text{Cu}]2$ (▒), $[^{64}\text{Cu}]3$ (■), and $[^{64}\text{Cu}]4$ (■).

3.8. PET Imaging

Overall, the BxPC-3 tumors were clearly visualized by PET imaging with both peptides at all time points (Figure 6); the PET imaging also showed that $[^{64}\text{Cu}]2$ provided the clearest images based on its superior tumor-to-background ratios. Most notably, as previously discussed for the biodistribution data, the PET images for $[^{64}\text{Cu}]1$ had much higher kidney accumulation and higher levels of radiation in the liver, indicative of possible *in vivo* instability of $[^{64}\text{Cu}]1$, which had shown substantially higher degradation in mouse serum compared to $[^{64}\text{Cu}]2$.

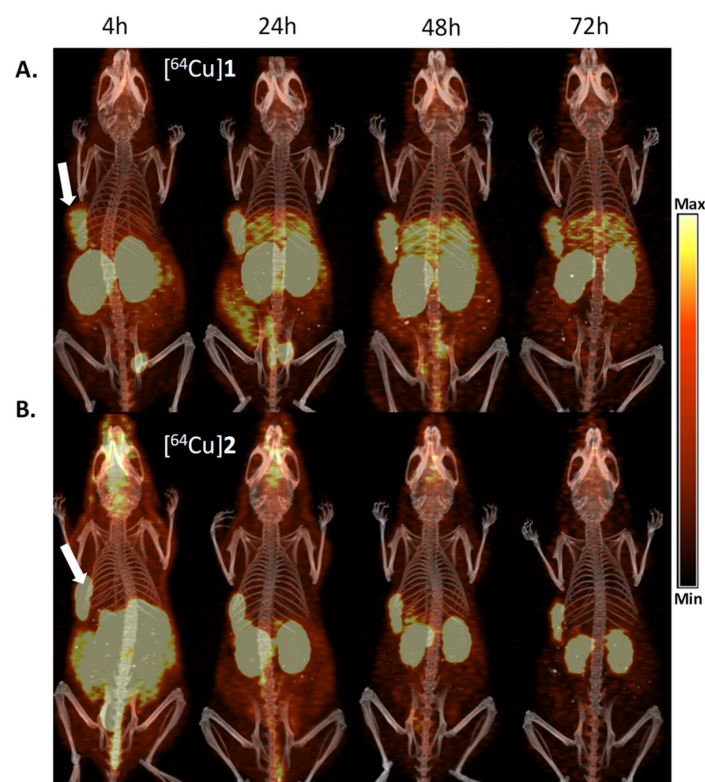


Figure 6. PET/CT imaging. Representative whole-body coronal maximum intensity projections (MIPs) of PET/CT images of mice bearing BxPC-3 xenograft tumors at 4 h, 24 h, 48 h, and 72 h p.i. of (A) $[^{64}\text{Cu}]1$ and (B) $[^{64}\text{Cu}]2$. Arrow: tumor. Decay corrected PET data are shown in color, CT data in gray.

4. Discussion

Cancer remains a leading cause of death globally [48,49]. Many cancers exhibit high expression of the cell surface receptor integrin $\alpha_v\beta_6$, and expression levels correlate with poor prognosis and reduced progression-free and overall survival [31,32,38]. Therefore, integrin $\alpha_v\beta_6$ has been identified as an important target both for imaging and treatment [50,51]. Receptor targeted delivery of radiopharmaceuticals is an important part of new approaches for improved cancer detection and therapy [48]. Peptides are attractive radiopharmaceuticals for both detection and treatment, because they are readily synthesized and can be chemically modified to optimize pharmacokinetics and metabolic stability. The addition of albumin binding moieties (ABMs) to numerous radiopharmaceuticals has demonstrated increased circulation time, reduced kidney uptake, and substantially increased tumor accumulation [18,52,53]. However, differences in the chemical structures of the ABM have been found at times to significantly affect the biodistribution, which ultimately determines target uptake, therapeutic efficacy, and off-target toxicity [52,54–56]. Thus, evaluation of different ABMs is important for optimal radiopharmaceutical performance towards the development of an $\alpha_v\beta_6$ -targeted radiotherapeutic agent. Our laboratory continues to develop integrin $\alpha_v\beta_6$ -targeting radiopharmaceuticals, including optimization of the core peptide structure [30] via PEGylation [14], and most recently the addition of an 4-(*p*-iodophenyl)butyryl (IP) ABM, which has demonstrated improved accumulation in tumors for both the [^{18}F]AIF-NOTA and [^{64}Cu]Cu-DOTA radiolabeled IP-ABM- $\alpha_v\beta_6$ -BP compared to the parent non-ABM $\alpha_v\beta_6$ -BP [42,44]. To further evaluate the choice of preferred ABM for $\alpha_v\beta_6$ -BP, the comparison of the IP-ABM with another prominent ABM, the Evans blue fragment (EB-ABM), was explored. The synthesis of both $\alpha_v\beta_6$ -BP peptides containing different ABMs, [^{64}Cu]1 or [^{64}Cu]2 (Scheme 1), was done efficiently using a solid-phase approach, which allowed installation of the respective ABM-peptide from the same batch of peptidyl-resin by first coupling an orthogonally protected lysine allowing for the attachment of the DOTA-chelator at the *N*-terminus and either the EB-ABM 8 or the IP-ABM at the sidechain. The IP-ABM included an aspartate (D) residue as it is reported to result in better tumor retention [28]. After removal from the resin and purification, both DOTA-ABM- $\alpha_v\beta_6$ -BP peptides (1 and 2) were efficiently radiolabeled with copper-64 to yield [^{64}Cu]1 and [^{64}Cu]2 in high radiochemical purity >97%.

The ABM containing peptides [^{64}Cu]1 and [^{64}Cu]2 both demonstrated high tumor uptake at 4 h p.i., over 5% and 7.5% ID/g, respectively; representing a greater than 3- to 4.5-fold increase, respectively, from the non-ABM bearing [^{64}Cu]Cu-DOTA- $\alpha_v\beta_6$ -BP ($1.61 \pm 0.70\%$ ID/g) [44]. The improvement in tumor accumulation was greater for the IP-ABM peptide [^{64}Cu]2 than for the EB-ABM peptide [^{64}Cu]1, and was in concordance with the cell binding to both DX3puro β_6 and BxPC-3 cells (Figure 2). Furthermore, the prolonged tumor uptake and retention (Figure 4A) were maintained for 72 h, and, in conjunction with rapid renal clearance, provided a high tumor-to-background ratio (Figure 5) and high contrast PET-images (Figure 6). Since the only difference between [^{64}Cu]1 and [^{64}Cu]2 is the ABM, and [^{64}Cu]2 showed significantly higher stability in serum compared to [^{64}Cu]1 (Figure 3), the observed differences in the tumor-to-background ratios could be attributed to the improved stability. This study adds to the growing number of literature reports describing improved tumor uptake following the incorporation of ABMs [4,7,11]. For example, the small molecule PSMA-617, a radiopharmaceutical targeting the prostate specific membrane antigen (PSMA), exhibited approximately a fivefold increase in tumor accumulation with the addition of an EB-ABM at 4 h and a twofold increase for the IP-ABM modified PSMA-617, compared to the unmodified (non-ABM bearing) PSMA-617; furthermore, the EB-ABM PSMA-617 maintained tumor accumulation over time (65.6–77.3% ID/g from 4 h to 48 h) [55]. In another study with PSMA-617, the addition of the IP-ABM also resulted in twofold higher accumulation in tumor tissue as compared to the non-ABM containing PSMA-617 agent (non-ABM PSMA-617: 38% ID/g vs. IP-ABM PSMA-617: 75.7% ID/g at 24 h) [28,57]. Other small molecule PSMA agents modified with ABMs have also shown improvements in tumor accumulation, with the EB-ABM MCG

PSMA agent having around a fourfold increase in tumor accumulation (MCG non-ABM: 10.9% ID/g vs. MCG-ABM: 40.4% ID/g at 24 h) [53] and an IP-ABM PSMA agent CTT1403 exhibiting >18-fold improvement in tumor accumulation (CTT1401 non-ABM: 2.2% ID/g vs. CTT1403-ABM: 40% ID/g at 24 h [54]. The addition of ABMs to other small molecule radiopharmaceuticals has also been shown to improve tumor accumulation with the small molecule radioligand folic acid modified with the IP-ABM having a threefold increase in tumor accumulation (ABM: 19.5% ID/g vs. non-ABM: 7% ID/g at 24 h, p.i.) with a considerably lower kidney accumulation (ABM: 28% ID/g vs. non-ABM: 70% ID/g at 4 h) [52,58].

Aside from small molecule radiopharmaceuticals, substantial benefits from the addition of ABMs to peptide radiopharmaceuticals have been shown; for example, the large peptide exendin-4 (39 amino acids), which targets the glucagon-like peptide 1 (GLP-1) receptor, when modified with the IP-ABM, demonstrated an improved stability and a twofold increase in tumor accumulation at 4 h, along with reduced kidney retention by more than half [7,59]. The small five amino acid integrin $\alpha_v\beta_3$ targeting cyclic peptide (cRGDfK) modified with EB-ABM and radiolabeled as [^{64}Cu]Cu NOTA-EB-cRGDfK displayed a >16-fold improvement (vs. [^{64}Cu]Cu NOTA-cRGDfK) in tumor accumulation in a U87MG glioblastoma tumor model (with ABM: 16.6% ID/g vs. non-ABM: <1.1% ID/g), but only had about a fivefold improvement in MDA-MB-435 melanoma and HT29 colorectal adenocarcinoma models [18]. The somatostatin receptor targeting peptide octreotide (TATE), which is eight amino acids in size, has seen some of the greatest improvements in tumor accumulation upon modification with an ABM. For example, the EB-ABM modified [^{177}Lu]Lu DOTA-EB-TATE provided a greater than eightfold increase in the tumor accumulation at 24 h (with ABM: 78.8% ID/g vs. non-ABM: 9.3% ID/g, respectively) [60] and the [^{86}Y]Y DOTA-EB-TATE showed a larger enhancement with a between 30- and 60-fold increase in tumor accumulation compared to [^{86}Y]Y DOTA-TATE, depending on the tumor model [6]. These studies paved the way for clinical trials where [^{177}Lu]Lu DOTA-EB-TATE showed an extended circulation which led to a 7.9-fold increase in tumor dose delivery [61]. Overall, these studies illustrate the potential benefits of including an ABM on targeted peptide receptor radionuclide therapy (PRRT).

The addition of either EB-ABM or the IP-ABM on the $\alpha_v\beta_6$ -BP did significantly increase tumor accumulation (three-to-fivefold from the non-ABM- $\alpha_v\beta_6$ -BP) and the overall clearance properties of the ABM-modified $\alpha_v\beta_6$ -BP peptides [^{64}Cu]1 and [^{64}Cu]2 were similar with predominantly renal excretion. The organ with the highest accumulation was the kidneys, with the initial kidney uptake of the EB-ABM peptide [^{64}Cu]1 having more than double that of the IP-ABM peptide [^{64}Cu]2 (4 h: $75.5 \pm 7.3\%$ ID/g vs. $33.6 \pm 5.4\%$ ID/g, $p = 0.0013$), with both dropping to approximately one third of their initial value at 72 h p.i. ($20.0 \pm 6.9\%$ ID/g and $11.4 \pm 1.0\%$ ID/g, respectively, $p = 0.10$, Figure 4). The introduction of the IP-ABM to the $\alpha_v\beta_6$ -BP significantly reduced kidney accumulation, which we hypothesize is due to the higher stability of the IP-ABM [^{64}Cu]2 over the EB-ABM [^{64}Cu]1. These data are promising and indicate that renal toxicity would be less of a concern for PRRT of $\alpha_v\beta_6$ -BP agents using the IP-ABM. The observed effects of the different ABMs on kidney uptake and retention are comparable to other radiopharmaceutical ABM-adducts, for example, the ABM modified peptide [^{177}Lu]Lu DOTA-TATE showed that the IP-ABM-analogue also provided lower kidney accumulation that was more rapidly cleared (dropping from $\sim 20\%$ ID/g at 4 h to $\sim 5\%$ ID/g at 72 h) compared to the EB-ABM-analogue ($\sim 30\%$ ID/g at 4 h to $\sim 15\%$ ID/g at 72 h) [29,60]. This similar kidney accumulation and retention trend was also observed with the small molecule PSMA-617 agent, where the EB-PSMA-617 had considerably higher kidney accumulation and retention compared to the IP-PSMA-617, which had rapid kidney clearance (EB-PSMA-617: $>20\%$ ID/g at 4 h, which remained at 48 h vs. IP-ABM-PSMA-617: $\sim 10\%$ ID/g at 4 h dropping to $<5\%$ ID/g at 48 h) [55]. Both [^{64}Cu]1 and [^{64}Cu]2 also displayed some secondary clearance through the gastrointestinal (GI) tract and excretion of radioactivity in the feces (Figures S20 and S21). The IP-ABM modified peptide [^{64}Cu]2 had higher GI accumulation, with the highest

uptake in the stomach of $18.1 \pm 2.9\%$ ID/g at 4 h, though, gratifyingly, both peptide's GI accumulation dropped down to less than one-fifth of their respective original value ($\leq 3.2\%$ ID/g at 72 h, Figure 4).

The non- $\alpha_v\beta_6$ -targeting ABM controls [^{64}Cu]3 and [^{64}Cu]4 were used to evaluate non-specific uptake and demonstrate that the enhanced tumor accumulation of [^{64}Cu]1 or [^{64}Cu]2 resulted from integrin $\alpha_v\beta_6$ receptor mediated uptake, as opposed to the enhanced permeability and retention (EPR) effect. As expected, [^{64}Cu]3 and [^{64}Cu]4 largely remained in the blood, thus mostly acting as blood pool imaging agents with high blood accumulation of 39.0% ID/g and 9.5% ID/g, respectively, at 4 h (Figure S25) and mirrored other similar non-targeted ABMs, such as the EB-ABM compound [^{64}Cu]Cu NOTA-EB (NEB, $\sim 15\%$ ID/g at 4 h, dropping to $\sim 10\%$ ID/g at 1 d) [16,23]. Compared to the ABM peptides [^{64}Cu]1 and [^{64}Cu]2, accumulation of [^{64}Cu]3 and [^{64}Cu]4 generally increased in organs with high blood flow (viz. heart, liver, and lungs; Figure 5A) but was lower in the kidneys (though the EB compound was still higher than the IP compound with 18.6% ID/g and 4.3% ID/g, respectively, at 4 h; Figure 5A), highlighting the effect of both the properties of the ABM as well as the targeting peptide moiety on kidney uptake. Both non-targeted [^{64}Cu]3 and [^{64}Cu]4, due to their much higher blood accumulation (>9 – 39 -fold higher than [^{64}Cu]1 and [^{64}Cu]2) and longer blood residence time, provided much higher tumor accumulation at 4 h than the two peptides [^{64}Cu]1 and [^{64}Cu]2 (Figure 5A). However, the non-targeted [^{64}Cu]3 and [^{64}Cu]4 showed minimal binding ($<4.3\%$) in cell binding studies to both the $\alpha_v\beta_6$ -expressing and $\alpha_v\beta_6$ -null cells (Figure S24), thus their higher tumor accumulation compared to [^{64}Cu]1 and [^{64}Cu]2 was attributed to the EPR effect (which, together with the long circulation, resulted in the expectedly low tumor-to-blood ratios of $<0.9/1$ (Figure 5B, Figure S26). By comparison, [^{64}Cu]1 and [^{64}Cu]2 showed high and $\alpha_v\beta_6$ -dependent cell binding (>30 – 60% binding; $\sim 20:1$ for DX3puro β_6 (+)/DX3puro (–) cells), and in vivo tumor uptake was efficiently blocked by the pre-administration of metal free 1 and 2, respectively, supporting integrin $\alpha_v\beta_6$ -dependent tumor accumulation (Figure S23). Taken together, the tumor uptake observed for the integrin $\alpha_v\beta_6$ -binding peptides [^{64}Cu]1 and [^{64}Cu]2 was attributed to specific targeting of the integrin $\alpha_v\beta_6$ receptor. Both ABM modified $\alpha_v\beta_6$ -BP peptides had improved pharmacokinetic profiles from the parent peptide and overall [^{64}Cu]2 demonstrated a more favorable biodistribution. Tumor retention of [^{64}Cu]1 and [^{64}Cu]2 was good over the three day study period, with each retaining about two-thirds of the original (4 h) uptake at 72 h p.i. The PET image quality improved, most notably for [^{64}Cu]2 over time after the initial uptake period (i.e., after 24 h p.i.) as a result of faster washout from non-target tissues (Figure 6). The high absolute tumor uptake of [^{64}Cu]2, its efficient binding and internalization to $\alpha_v\beta_6$ -expressing cells (Figure 2), and its better serum stability (Figure 3) demonstrate the potential of using the [^{64}Cu]2 as an integrin $\alpha_v\beta_6$ -targeted peptide receptor radionuclide therapy (PRRT) agent where the copper-64 is replaced by a therapeutic radioisotope such as lutetium-177.

5. Conclusions

The effect of Evans blue (EB) and 4-(*p*-iodophenyl)butyryl (IP)-based albumin binding moieties (ABMs) on the pharmacokinetics of $\alpha_v\beta_6$ -BP, a peptide targeting the cancer-associated cell surface receptor integrin $\alpha_v\beta_6$ was investigated. The albumin binding moieties on $\alpha_v\beta_6$ -BP did not interfere with integrin $\alpha_v\beta_6$ affinity or selectivity in vitro. In vivo in a BxPC-3 pancreatic tumor xenograft mouse model, the IP-ABM-modified $\alpha_v\beta_6$ -BP [^{64}Cu]2 had a considerably more favorable pharmacokinetic profile compared to the EB-ABM-modified $\alpha_v\beta_6$ -BP [^{64}Cu]1, with higher tumor uptake, reduced kidney and liver uptake, and improved tumor-to-background ratios that led to a clearer tumor visualization by PET imaging. Furthermore, the IP-ABM-modified $\alpha_v\beta_6$ -BP [^{64}Cu]2 had superior serum stability, making it a lead candidate for future integrin $\alpha_v\beta_6$ -targeted imaging and therapy studies.

Supplementary Materials: The following are available online at <https://www.mdpi.com/article/10.3390/pharmaceutics14040745/s1>, S1–S26. Table S1–S3: Table of Contents, Table S3: RP-HPLC methods, Figure S4: Schematic for solid phase reaction of EB-ABM **8** to peptidyl resin of DOTA-K(NH₂- $\alpha_v\beta_6$ -BP to produce DOTA-EB- $\alpha_v\beta_6$ -BP **1** after cleavage and pictorial of the reaction of **8** with peptidyl resin of DOTA-K(NH₂)- $\alpha_v\beta_6$ -BP, Figure S5: RP-HPLC and MALDI-TOF of DOTA-EB- $\alpha_v\beta_6$ -BP **1**, Figure S6: Radio-RP-HPLC of [⁶⁴Cu]**1** and co-injection radio-RP-HPLC of [^{Nat}Cu]**1** and [⁶⁴Cu]**1**, Figure S7: MALDI-TOF of [^{Nat}Cu]**1**, Figure S8: RP-HPLC and MALDI-TOF of DOTA-IP- $\alpha_v\beta_6$ -BP **2**, Figure S9: Radio-RP-HPLC of [⁶⁴Cu]**2** and co-injection radio-RP-HPLC of [^{Nat}Cu]**2** and [⁶⁴Cu]**2**, Figure S10: MALDI-TOF of [^{Nat}Cu]**2**, Figure S11: RP-HPLC and MALDI-TOF of DOTA-EB-ABM **3**, Figure S12: Radio-RP-HPLC of [⁶⁴Cu]**3** and co-injection radio-RP-HPLC of [^{Nat}Cu]**3** and [⁶⁴Cu]**3**, Figure S13: MALDI-TOF of [^{Nat}Cu]**3**, Figure S14: RP-HPLC and MALDI-TOF of DOTA-IP-ABM **4**, Figure S15: Radio-RP-HPLC of [⁶⁴Cu]**4** and co-injection radio-RP-HPLC of [^{Nat}Cu]**4** and [⁶⁴Cu]**4**, Figure S16: MALDI-TOF of [^{Nat}Cu]**4**, Figure S17: RP-HPLC and ESI-FTMS of compound **6**, Figure S18: RP-HPLC and ESI-FTMS of EB-ABM **8**, Figure S19: ¹H NMR and COSY of EB-ABM **8**, Figure S20: Biodistribution of [⁶⁴Cu]**1**, Figure S21: Biodistribution of [⁶⁴Cu]**2**, Figure S22: Tumor-to-organ ratios from 4 h to 72 h p.i. of [⁶⁴Cu]**1** and [⁶⁴Cu]**2**, Figure S23: Blocking biodistribution of [⁶⁴Cu]**1** and [⁶⁴Cu]**2**, Figure S24: Cell binding assay for [⁶⁴Cu]**3** and [⁶⁴Cu]**4**, Figure S25: Biodistribution of [⁶⁴Cu]**3** and [⁶⁴Cu]**4**, Figure S26: Summary of Tumor-to-organ ratios at 4 h for [⁶⁴Cu]**1–4**.

Author Contributions: Conceptualization, J.L.S. and R.A.D.; methodology, R.A.D. and S.H.H.; formal analysis, J.L.S., R.A.D. and S.H.H.; synthesis and radiolabeling with copper-64, R.A.D.; compound characterization and purification and formulation, R.A.D.; serum stability assay, R.A.D.; cell culture, R.H.; cell binding assay and serum binding assays, S.H.H. and R.A.D.; biodistribution, S.H.H., R.H. and R.A.D.; resources, J.L.S.; data curation, R.A.D.; writing—original draft preparation, R.A.D.; writing—review and editing, R.A.D., J.L.S. and S.H.H.; supervision, J.L.S.; funding acquisition, J.L.S. All authors have read and agreed to the published version of the manuscript.

Funding: This research was funded by National Institutes of Health’s National Cancer Institute, grants number R01CA199725 and R50CA211556-01.

Institutional Review Board Statement: Radioactive work was conducted under radioactive use authorization 9098 managed by University of California, Davis Radiation Safety Services. All animal and biological research were conducted under biological use authorization R1580 and all animal work was conducted in accordance with procedures pre-approved by the Institutional of Animal Care and Use Committee (IACUC) at the University of California, Davis which is regulated by several independent resources. Accreditation and oversight has been approved since 1966 by AAALAC #000029 and by the Office of Laboratory Animal Welfare (OLAW) #D16-00272 (A3433-01).

Informed Consent Statement: Not applicable.

Data Availability Statement: Additional data supporting the reported results can be found in the Supplementary Materials (S1–S26).

Acknowledgments: We would like to thank the Center for Molecular and Genomic Imaging at UC Davis, Charles Smith and Sarah Tam for their technical support of injections during animal studies and running of the PET/CT scanners.

Conflicts of Interest: The authors declare the following competing financial interest(s): S. H. Hausner is a co-inventor of intellectual property related to $\alpha_v\beta_6$ -BP. J. L. Sutcliffe is founder and CEO of and holds ownership interest (including patents) in Luminance Biosciences, Inc., and is a co-inventor of intellectual property related to $\alpha_v\beta_6$ -BP. The funding agencies had no role in the design of the study; in the collection, analyses, or interpretation of data; in the writing of the manuscript, or in the decision to publish the results.

References

1. Davis, R.A.; Hausner, S.H.; Sutcliffe, J.L. Peptides as radiopharmaceutical vectors. In *Radiopharmaceutical Chemistry*; Lewis, J.S., Windhorst, A.D., Zeglis, B.M., Eds.; Springer International Publishing: Cham, Switzerland, 2019; pp. 137–162.
2. Trier, N.; Hansen, P.; Houen, G. Peptides, antibodies, peptide antibodies and more. *Int. J. Mol. Sci.* **2019**, *20*, 6289. [[CrossRef](#)] [[PubMed](#)]
3. Kręcisz, P.; Czarnecka, K.; Królicki, L.; Mikiciuk-Olasik, E.; Szymański, P. Radiolabeled peptides and antibodies in medicine. *Bioconjugate Chem.* **2021**, *32*, 25–42. [[CrossRef](#)] [[PubMed](#)]

4. Zorzi, A.; Linciano, S.; Angelini, A. Non-covalent albumin-binding ligands for extending the circulating half-life of small biotherapeutics. *Med. Chem. Commun.* **2019**, *10*, 1068–1081. [[CrossRef](#)] [[PubMed](#)]
5. Zorzi, A.; Middendorp, S.J.; Wilbs, J.; Deyle, K.; Heinis, C. Acylated heptapeptide binds albumin with high affinity and application as tag furnishes long-acting peptides. *Nat. Commun.* **2017**, *8*, 16092. [[CrossRef](#)] [[PubMed](#)]
6. Tian, R.; Jacobson, O.; Niu, G.; Kiesewetter, D.O.; Wang, Z.; Zhu, G.; Ma, Y.; Liu, G.; Chen, X. Evans blue attachment enhances somatostatin receptor subtype-2 imaging and radiotherapy. *Theranostics* **2018**, *8*, 735–745. [[CrossRef](#)]
7. Chen, H.; Wang, G.; Lang, L.; Jacobson, O.; Kiesewetter, D.O.; Liu, Y.; Ma, Y.; Zhang, X.; Wu, H.; Zhu, L.; et al. Chemical conjugation of Evans blue derivative: A strategy to develop long-acting therapeutics through albumin binding. *Theranostics* **2016**, *6*, 243–253. [[CrossRef](#)]
8. Dennis, M.S.; Zhang, M.; Meng, G.Y.; Kadkhodayan, M.; Kirchhofer, D.; Combs, D.; Damico, L.A. Albumin binding as a general strategy for improving the pharmacokinetics of proteins. *J. Biol. Chem.* **2002**, *277*, 35035–35043. [[CrossRef](#)]
9. Jacobson, O.; Kiesewetter, D.O.; Chen, X. Albumin-binding Evans blue derivatives for diagnostic imaging and production of long-acting therapeutics. *Bioconjugate Chem.* **2016**, *27*, 2239–2247. [[CrossRef](#)]
10. Lau, J.; Jacobson, O.; Niu, G.; Lin, K.-S.; Bénard, F.; Chen, X. Bench to bedside: Albumin binders for improved cancer radioligand therapies. *Bioconjugate Chem.* **2019**, *30*, 487–502. [[CrossRef](#)]
11. Brandt, M.; Cardinale, J.; Giammei, C.; Guarrochena, X.; Happl, B.; Jouini, N.; Mindt, T.L. Mini-review: Targeted radiopharmaceuticals incorporating reversible, low molecular weight albumin binders. *Nucl. Med. Biol.* **2019**, *70*, 46–52. [[CrossRef](#)]
12. Gao, H.; Luo, C.; Yang, G.; Du, S.; Li, X.; Zhao, H.; Shi, J.; Wang, F. Improved in vivo targeting capability and pharmacokinetics of ^{99m}Tc-labeled isoDGR by dimerization and albumin-binding for glioma imaging. *Bioconjugate Chem.* **2019**, *30*, 2038–2048. [[CrossRef](#)] [[PubMed](#)]
13. Cheng, T.-L.; Chuang, K.-H.; Chen, B.-M.; Roffler, S.R. Analytical measurement of PEGylated molecules. *Bioconjugate Chem.* **2012**, *23*, 881–899. [[CrossRef](#)] [[PubMed](#)]
14. Hausner, S.H.; Bauer, N.; Hu, L.Y.; Knight, L.M.; Sutcliffe, J.L. The effect of bi-terminal PEGylation of an integrin $\alpha_v\beta_6$ -targeted ¹⁸F peptide on pharmacokinetics and tumor uptake. *J. Nucl. Med.* **2015**, *56*, 784–790. [[CrossRef](#)] [[PubMed](#)]
15. Müller, C.; Farkas, R.; Borgna, F.; Schmid, R.M.; Benešová, M.; Schibli, R. Synthesis, radiolabeling, and characterization of plasma protein-binding ligands: Potential tools for modulation of the pharmacokinetic properties of (radio) pharmaceuticals. *Bioconjugate Chem.* **2017**, *28*, 2372–2383. [[CrossRef](#)] [[PubMed](#)]
16. Liu, Z.; Chen, X. Simple bioconjugate chemistry serves great clinical advances: Albumin as a versatile platform for diagnosis and precision therapy. *Chem. Soc. Rev.* **2016**, *45*, 1432–1456. [[CrossRef](#)]
17. Niu, G.; Lang, L.; Kiesewetter, D.O.; Ma, Y.; Sun, Z.; Guo, N.; Guo, J.; Wu, C.; Chen, X. In vivo labeling of serum albumin for PET. *J. Nucl. Med.* **2014**, *55*, 1150–1156. [[CrossRef](#)]
18. Chen, H.; Jacobson, O.; Niu, G.; Weiss, I.D.; Kiesewetter, D.O.; Liu, Y.; Ma, Y.; Wu, H.; Chen, X. Novel “add-on” molecule based on Evans blue confers superior pharmacokinetics and transforms drugs to theranostic agents. *J. Nucl. Med.* **2017**, *58*, 590–597. [[CrossRef](#)]
19. Ehlerding, E.B.; Lan, X.; Cai, W. Albumin hitchhiking” with an Evans blue analog for cancer theranostics. *Theranostics* **2018**, *8*, 812–814. [[CrossRef](#)]
20. Liu, Y.; Wang, G.; Zhang, H.; Ma, Y.; Lang, L.; Jacobson, O.; Kiesewetter, D.O.; Zhu, L.; Gao, S.; Ma, Q.; et al. Stable Evans blue derived extendin-4 peptide for type 2 diabetes treatment. *Bioconjugate Chem.* **2016**, *27*, 54–58. [[CrossRef](#)]
21. Saunders, N.R.; Dziegielewska, K.M.; Møllgård, K.; Habgood, M.D. Markers for blood-brain barrier integrity: How appropriate is Evans blue in the twenty-first century and what are the alternatives? *Front. Neurosci.* **2015**, *9*, 385. [[CrossRef](#)]
22. Yamamoto, T.; Ikuta, K.; Oi, K.; Abe, K.; Uwatoku, T.; Murata, M.; Shigetani, N.; Yoshimitsu, K.; Shimokawa, H.; Katayama, Y. First functionalized MRI contrast agent recognizing vascular lesions. *Anal. Sci.* **2004**, *20*, 5–7. [[CrossRef](#)] [[PubMed](#)]
23. Zhang, J.; Lang, L.; Zhu, Z.; Li, F.; Niu, G.; Chen, X. Clinical translation of an albumin-binding PET radiotracer ⁶⁸Ga-NEB. *J. Nucl. Med.* **2015**, *56*, 1609–1614. [[CrossRef](#)] [[PubMed](#)]
24. Zhang, F.; Xue, J.; Shao, J.; Jin, L. Compilation of 222 drugs’ plasma protein binding data and guidance for study designs. *Drug Discov. Today* **2012**, *17*, 475–485. [[CrossRef](#)] [[PubMed](#)]
25. Wang, Y.; Lang, L.; Huang, P.; Wang, Z.; Jacobson, O.; Kiesewetter, D.O.; Ali, I.U.; Teng, G.; Niu, G.; Chen, X. In vivo albumin labeling and lymphatic imaging. *Proc. Natl. Acad. Sci. USA* **2015**, *112*, 208–213. [[CrossRef](#)]
26. Yao, L.; Xue, X.; Yu, P.; Ni, Y.; Chen, F. Evans blue dye: A revisit of its applications in biomedicine. *Contrast Media Mol. Imaging.* **2018**, *2018*, 10. [[CrossRef](#)]
27. Dumelin, C.E.; Trüssel, S.; Buller, F.; Trachsel, E.; Bootz, F.; Zhang, Y.; Mannocci, L.; Beck, S.C.; Drumea-Mirancea, M.; Seeliger, M.W.; et al. A portable albumin binder from a DNA-encoded chemical library. *Angew. Chem. Int. Ed.* **2008**, *47*, 3196–3201. [[CrossRef](#)] [[PubMed](#)]
28. Umbricht, C.A.; Benešová, M.; Schibli, R.; Müller, C. Preclinical development of novel PSMA-targeting radioligands: Modulation of albumin-binding properties to improve prostate cancer therapy. *Mol. Pharm.* **2018**, *15*, 2297–2306. [[CrossRef](#)]
29. Rousseau, E.; Lau, J.; Zhang, Z.; Uribe, C.F.; Kuo, H.-T.; Zhang, C.; Zeisler, J.; Colpo, N.; Lin, K.-S.; Bénard, F. Effects of adding an albumin binder chain on [¹⁷⁷Lu]Lu-DOTATATE. *Nucl. Med. Biol.* **2018**, *66*, 10–17. [[CrossRef](#)]

30. Hausner, S.H.; Bold, R.J.; Cheuy, L.Y.; Chew, H.K.; Daly, M.E.; Davis, R.A.; Foster, C.C.; Kim, E.J.; Sutcliffe, J.L. Preclinical development and first-in human imaging of integrin $\alpha_v\beta_6$ -binding peptide in metastatic carcinoma. *Clinic. Cancer Res.* **2019**, *25*, 1206–1215. [[CrossRef](#)]
31. Wang, B.; Wang, W.; Niu, W.; Liu, E.; Liu, X.; Wang, J.; Peng, C.; Liu, S.; Xu, L.; Wang, L.; et al. SDF-1/CXCR4 axis promotes directional migration of colorectal cancer cells through upregulation of integrin $\alpha_v\beta_6$. *Carcinogenesis* **2013**, *35*, 282–291. [[CrossRef](#)]
32. Li, Z.; Lin, P.; Gao, C.; Peng, C.; Liu, S.; Gao, H.; Wang, B.; Wang, J.; Niu, J.; Niu, W. Integrin β_6 acts as an unfavorable prognostic indicator and promotes cellular malignant behaviors via ERK-ETS1 pathway in pancreatic ductal adenocarcinoma (PDAC). *Tumor Biol.* **2016**, *37*, 5117–5131. [[CrossRef](#)] [[PubMed](#)]
33. Izabela, L.; Jacek, M. Integrins as a new target for cancer treatment. *Anti-Cancer Agents Med. Chem.* **2019**, *19*, 580–586.
34. Bandyopadhyay, A.; Raghavan, S. Defining the role of integrin $\alpha_v\beta_6$ in cancer. *Curr. Drug Targets.* **2009**, *10*, 645–652. [[CrossRef](#)]
35. Ahmed, N.; Pansino, F.; Clyde, R.; Murthi, P.; Quinn, M.A.; Rice, G.E.; Agrez, M.V.; Mok, S.; Baker, M.S. Overexpression of $\alpha_v\beta_6$ integrin in serous epithelial ovarian cancer regulates extracellular matrix degradation via the plasminogen activation cascade. *Carcinogenesis* **2002**, *23*, 237–244. [[CrossRef](#)]
36. Elayadi, A.N.; Samli, K.N.; Prudkin, L.; Liu, Y.-H.; Bian, A.; Xie, X.-J.; Wistuba, I.I.; Roth, J.A.; McGuire, M.J.; Brown, K.C. A peptide selected by biopanning identifies the integrin $\alpha_v\beta_6$ as a prognostic biomarker for nonsmall cell lung cancer. *Cancer Res.* **2007**, *67*, 5889–5895. [[CrossRef](#)] [[PubMed](#)]
37. Moore, K.M.; Thomas, G.J.; Duffy, S.W.; Warwick, J.; Gabe, R.; Chou, P.; Ellis, I.O.; Green, A.R.; Haider, S.; Brouillette, K.; et al. Therapeutic targeting of integrin $\alpha_v\beta_6$ in breast cancer. *J. Natl. Cancer Inst.* **2014**, *106*, 1–14. [[CrossRef](#)]
38. Zhang, Z.Y.; Xu, K.S.; Wang, J.S.; Yang, G.Y.; Wang, W.; Wang, J.Y.; Niu, W.B.; Liu, E.Y.; Mi, Y.T.; Niu, J. Integrin $\alpha_v\beta_6$ acts as a prognostic indicator in gastric carcinoma. *Clin. Oncol.* **2008**, *20*, 61–66. [[CrossRef](#)]
39. Hsiao, J.-R.; Chang, Y.; Chen, Y.-L.; Hsieh, S.-H.; Hsu, K.-F.; Wang, C.-F.; Tsai, S.-T.; Jin, Y.-T. Cyclic $\alpha_v\beta_6$ -targeting peptide selected from biopanning with clinical potential for head and neck squamous cell carcinoma. *Head Neck.* **2010**, *32*, 160–172. [[PubMed](#)]
40. Bates, R.C. The $\alpha_v\beta_6$ integrin as a novel molecular target for colorectal cancer. *Future Oncol.* **2005**, *1*, 821–828. [[CrossRef](#)]
41. Berghoff, A.S.; Kovanda, A.K.; Melchardt, T.; Bartsch, R.; Hainfellner, J.A.; Sipos, B.; Schittenhelm, J.; Zielinski, C.C.; Widhalm, G.; Dieckmann, K.; et al. $\alpha_v\beta_3$, $\alpha_v\beta_5$ and $\alpha_v\beta_6$ integrins in brain metastases of lung cancer. *Clin. Exper. Met.* **2014**, *31*, 841–851. [[CrossRef](#)]
42. Hausner, S.H.; Bauer, N.; Davis, R.A.; Ganguly, T.; Tang, S.Y.C.; Sutcliffe, J.L. The effects of an albumin binding moiety on the targeting and pharmacokinetics of an integrin $\alpha_v\beta_6$ -selective peptide labeled with aluminum [^{18}F]fluoride. *Mol. Imaging Biol.* **2020**, *22*, 1543–1552. [[CrossRef](#)] [[PubMed](#)]
43. Hausner, S.H.; Bauer, N.; Sutcliffe, J.L. In vitro and in vivo evaluation of the effects of aluminum [^{18}F]fluoride radiolabeling on an integrin $\alpha_v\beta_6$ -specific peptide. *Nucl. Med. Biol.* **2014**, *41*, 43–50. [[CrossRef](#)] [[PubMed](#)]
44. Ganguly, T.; Bauer, N.; Davis, R.A.; Hausner, S.H.; Tang, S.Y.; Sutcliffe, J.L. Evaluation of copper-64-labeled $\alpha_v\beta_6$ -targeting peptides: Addition of an albumin binding moiety to improve pharmacokinetics. *Mol. Pharm.* **2021**, *18*, 4437–4447. [[CrossRef](#)] [[PubMed](#)]
45. Zhang, F.; Zhu, G.; Jacobson, O.; Liu, Y.; Chen, K.; Yu, G.; Ni, Q.; Fan, J.; Yang, Z.; Xu, F.; et al. Transformative nanomedicine of an amphiphilic camptothecin prodrug for long circulation and high tumor uptake in cancer therapy. *ACS Nano.* **2017**, *11*, 8838–8848. [[CrossRef](#)]
46. Favre-Besse, F.-C.; Poirel, O.; Bersot, T.; Kim-Grellier, E.; Daumas, S.; El Mestikawy, S.; Acher, F.C.; Pietrancosta, N. Design, synthesis and biological evaluation of small-azo-dyes as potent vesicular glutamate transporters inhibitors. *Eur. J. Med. Chem.* **2014**, *78*, 236–247. [[CrossRef](#)] [[PubMed](#)]
47. Tang, Y.C.; Davis, R.A.; Ganguly, T.; Sutcliffe, J.L. Identification, characterization, and optimization of integrin $\alpha_v\beta_6$ -targeting peptides from a one-bead one-compound (OBOC) library: Towards the development of positron emission tomography (PET) imaging agents. *Molecules* **2019**, *24*, 309. [[CrossRef](#)]
48. Padma, V.V. An overview of targeted cancer therapy. *BioMedicine* **2015**, *5*, e46. [[CrossRef](#)]
49. Siegel, R.L.; Miller, K.D.; Jemal, A. Cancer statistics. *CA Cancer J. Clin.* **2019**, *69*, 7–34. [[CrossRef](#)]
50. Willemieke, T.S.; Farina-Sarasquota, A.; Boonstra, M.C.; Prevoo, H.A.; Sier, C.F.; Mieog, J.S.; Morreau, J.; van Eijck, C.H.; Kuppen, P.J.; van de Velde, C.J.; et al. Selection of optimal molecular targets for tumor-specific imaging in pancreatic ductal adenocarcinoma. *Oncotarget* **2017**, *8*, 56816–56828.
51. Färber, S.F.; Wurzer, A.; Reichart, F.; Beck, R.; Kessler, H.; Wester, H.-J.; Notni, J. Therapeutic radiopharmaceuticals targeting integrin $\alpha_v\beta_6$. *ACS Omega.* **2018**, *3*, 2428–2436. [[CrossRef](#)]
52. Müller, C.; Struthers, H.; Winiger, C.; Zhernosekov, K.; Schibli, R. DOTA conjugate with an albumin-binding entity enables the first folic acid-targeted ^{177}Lu -radionuclide tumor therapy in mice. *J. Nucl. Med.* **2013**, *54*, 124–131. [[CrossRef](#)] [[PubMed](#)]
53. Wang, Z.; Jacobson, O.; Tian, R.; Mease, R.C.; Kiesewetter, D.O.; Niu, G.; Pomper, M.G.; Chen, X. Radioligand therapy of prostate cancer with a long-lasting prostate-specific membrane antigen targeting agent ^{90}Y -DOTA-EB-MCG. *Bioconjugate Chem.* **2018**, *29*, 2309–2315. [[CrossRef](#)] [[PubMed](#)]
54. Choy, C.J.; Ling, X.; Geruntho, J.J.; Beyer, S.K.; Latoche, J.D.; Langton-Webster, B.; Anderson, C.J.; Berkman, C.E. ^{177}Lu -labeled phosphoramidate-based PSMA inhibitors: The effect of an albumin binder on biodistribution and therapeutic efficacy in prostate tumor-bearing mice. *Theranostics* **2017**, *7*, 1928–1939. [[CrossRef](#)] [[PubMed](#)]

55. Wang, Z.; Tian, R.; Niu, G.; Ma, Y.; Lang, L.; Szajek, L.P.; Kiesewetter, D.O.; Jacobson, O.; Chen, X. Single low-dose injection of Evans blue modified PSMA-617 radioligand therapy eliminates prostate-specific membrane antigen positive tumors. *Bioconjugate Chem.* **2018**, *29*, 3213–3221. [[CrossRef](#)] [[PubMed](#)]
56. Kuo, H.-T.; Lin, K.-S.; Zhang, Z.; Uribe, C.F.; Merkens, H.; Zhang, C.; Bénard, F. ¹⁷⁷Lu-labeled albumin-binder–conjugated PSMA-targeting agents with extremely high tumor uptake and enhanced tumor-to-kidney absorbed dose ratio. *J. Nucl. Med.* **2021**, *62*, 521–527. [[CrossRef](#)] [[PubMed](#)]
57. Benešová, M.; Umbricht, C.A.; Schibli, R.; Müller, C. Albumin-binding PSMA ligands: Optimization of the tissue distribution profile. *Mol. Pharm.* **2018**, *15*, 934–946. [[CrossRef](#)]
58. Siwowska, K.; Haller, S.; Bortoli, F.; Benešová, M.; Broehn, V.; Bernhardt, P.; Schibli, R.; Müller, C. Preclinical comparison of albumin-binding radiofolates: Impact of linker entities on the in vitro and in vivo properties. *Mol. Pharm.* **2017**, *14*, 523–532. [[CrossRef](#)]
59. Kaeppli, S.A.M.; Jodal, A.; Gotthardt, M.; Schibli, R.; Béhé, M. Exendin-4 derivatives with an albumin-binding moiety show decreased renal retention and improved GLP-1 receptor targeting. *Mol. Pharm.* **2019**, *16*, 3760–3769. [[CrossRef](#)]

60. Bandara, N.; Jacobson, O.; Mpoy, C.; Chen, X.; Rogers, B.E. Novel structural modification based on Evans blue dye to improve pharmacokinetics of a somatostatin-receptor-based theranostic agent. *Bioconjugate Chem.* **2018**, *29*, 2448–2454. [[CrossRef](#)]
61. Zhang, J.; Wang, H.; Jacobson, O.; Cheng, Y.; Niu, G.; Li, F.; Bai, C.; Zhu, Z.; Chen, X. Safety, pharmacokinetics, and dosimetry of a long-acting radiolabeled somatostatin analog ^{177}Lu -DOTA-EB-TATE in patients with advanced metastatic neuroendocrine tumors. *J. Nucl. Med.* **2018**, *59*, 1699–1705. [[CrossRef](#)]